Editors' Suggestion

Geometry of the set of quantum correlations

Koon Tong Goh,[1,*] Jędrzej Kaniewski,[2,†] Elie Wolfe,[3,‡] Tamás Vértesi,[4] Xingyao Wu,[5] Yu Cai,[1] Yeong-Cherng Liang,[6,§] and Valerio Scarani[1,7]

[1]*Centre for Quantum Technologies, National University of Singapore, Singapore 117543, Singapore*
[2]*QMATH, Department of Mathematical Sciences, University of Copenhagen, Universitetsparken 5, 2100 Copenhagen, Denmark*
[3]*Perimeter Institute for Theoretical Physics, Waterloo, Ontario N2L 2Y5, Canada*
[4]*Institute for Nuclear Research, Hungarian Academy of Sciences, Debrecen 4001, Hungary*
[5]*Joint Center for Quantum Information and Computer Science, University of Maryland, College Park, Maryland 20742, USA*
[6]*Department of Physics, National Cheng Kung University, Tainan 701, Taiwan*
[7]*Department of Physics, National University of Singapore, Singapore 117542, Singapore*

(Received 14 November 2017; published 7 February 2018)

It is well known that correlations predicted by quantum mechanics cannot be explained by any classical (local-realistic) theory. The relative strength of quantum and classical correlations is usually studied in the context of Bell inequalities, but this tells us little about the geometry of the quantum set of correlations. In other words, we do not have a good intuition about what the quantum set actually looks like. In this paper we study the geometry of the quantum set using standard tools from convex geometry. We find explicit examples of rather counterintuitive features in the simplest nontrivial Bell scenario (two parties, two inputs, and two outputs) and illustrate them using two-dimensional slice plots. We also show that even more complex features appear in Bell scenarios with more inputs or more parties. Finally, we discuss the limitations that the geometry of the quantum set imposes on the task of self-testing.

DOI: 10.1103/PhysRevA.97.022104

I. INTRODUCTION

Local measurements performed on entangled particles can give rise to correlations which are stronger than those present in any classical theory, a phenomenon known as Bell nonlocality. This seminal result, often referred to as Bell's theorem, was proven by Bell more than five decades ago [1] and the existence of such correlations has recently been confirmed unequivocally in a couple of technologically demanding experiments [2–5].

In addition to its fundamental significance, Bell nonlocality has also found real-life applications, notably in secure communication, generation of certifiably secure randomness, and more generally device-independent quantum information processing (see Ref. [6] for a review on Bell nonlocality and its applications). In the device-independent setting, we do not have a complete description of our physical setup and draw conclusions based only on the observed correlations instead. Thorough understanding of the sets of correlations allowed by different physical theories is thus essential to comprehend the power of device-independent quantum information processing.

In this language, Bell's theorem simply states that the set of correlations allowed by quantum theory $\mathcal{Q}$ is a *strict superset* of the set of correlations allowed by classical theories $\mathcal{L}$. The difference between these two objects is often investigated via *Bell inequalities*, i.e., linear constraints that must be satisfied by classical correlations but may be violated by quantum mechanics. Usual examples include the inequalities derived by Clauser, Horne, Shimony, and Holt (CHSH) [7] and Mermin [8].

Although quantum correlations may be stronger than their classical counterpart, they cannot be arbitrarily strong. In particular, they obey the no-signaling principle proposed by Popescu and Rohrlich [9]. Imposing this principle alone gives the no-signaling set $\mathcal{NS}$, which turns out to be a *strict superset* of $\mathcal{Q}$; i.e., we arrive at the following well-known strict inclusions:

$$\mathcal{L} \subsetneq \mathcal{Q} \subsetneq \mathcal{NS}. \tag{1}$$

Bell scenarios are parametrized by the number of inputs and outputs at each site. In this work, we assume that all these numbers are finite and then the local and no-signaling sets are polytopes, while the quantum set is a convex set but not a polytope. It is known that all of them span the same affine space, i.e., $\dim \mathcal{L} = \dim \mathcal{Q} = \dim \mathcal{NS}$ [10,11].

In the literature, the relation between the three sets is sometimes represented by a simple diagram which consists of a circle sandwiched between two squares similar to Fig. 2; see, e.g., Refs. [6,12]. While this picture accurately represents a particular two-dimensional slice (cross section) of the quantum set, it does not capture all the intricacies related to its geometry; see, e.g., Refs. [13–23]. The quantum set is arguably the most important object in the field of quantum correlations and, while some special subspaces are rather well understood [24–28], in general surprisingly little is known about its geometry [10] beyond the fact that it is convex [29]. In this work, we explore the unusual features of the quantum set and use standard notions from convex geometry to formalize them.

*ktgoh@u.nus.edu
†jkaniewski@math.ku.dk
‡ewolfe@perimeterinstitute.ca
§ycliang@mail.ncku.edu.tw

Understanding the geometry of the quantum set has immediate implications for (at least) two distinct lines of research.

The first one is related to the question of whether the quantum set admits a "physical description," i.e., whether there exists a simple, physically motivated principle which singles out precisely the quantum set without referring to operators acting on Hilbert spaces. Several such rules have been proposed [9,17,23,30–32] (the no-signaling principle being the first), but none of them has been shown to recover the quantum set. Checking whether these physical principles correctly reproduce the unusual features of the true quantum set, as was done in Refs. [16,17,19,30–32], will give us a better understanding of their strengths and weaknesses and might help us in the search of the correct physical principle.

The geometry of the quantum set is also related to the task of self-testing [10,24,33,34] in which we aim to deduce properties of the quantum system under consideration from the observed correlations alone. The fact that the geometry of the quantum set is more complex than that of the circle in Fig. 2 imposes concrete limitations on our ability to make self-testing statements, which we discuss in the relevant sections.

In Sec. II, we define the three correlation sets and propose a geometrically motivated classification of Bell functions. Sections III and IV contain examples of various unusual geometrical features of the quantum set. In Sec. V, we summarize the most important findings and discuss some open questions. In the appendixes, one can find (1) a simple proof that the quantum set in the simplest Bell scenario is closed, (2) connections between the CHSH Bell-inequality violation and some distance measures in the same Bell scenario, (3) further examples of unusual slices of the quantum set, (4) tools that we have developed to identify unusual quantum faces, (5) a proof that the optimal quantum distribution realizing the Hardy paradox [35] is not *exposed*, and (6) some other technical details of our results.

II. PRELIMINARIES

While discussing the geometry of the quantum set it is natural to employ standard tools from convex geometry, e.g., the notions of *exposed*, *extremal*, and *boundary* points. Let us recall that for a compact convex set $\mathcal{A}$ we have

$$\mathcal{A}_{\text{exp}} \subseteq \mathcal{A}_{\text{ext}} \subseteq \mathcal{A}_{\text{bnd}} \subseteq \mathcal{A} \tag{2}$$

and as shown in Fig. 1 these inclusions are in general strict. We will also use the notion of an *exposed face* of a convex set. A short and self-contained introduction to these notions can be found in Appendix A.

A. Three important correlation sets

Following the convention of Ref. [36], we denote the Bell scenario of n parties who (each) have m measurement settings with Δ possible outcomes by (n-m-Δ). In this work, we focus predominantly on the bipartite case, i.e., $n = 2$, and then the entire statistics can be assembled into a real vector $\vec{P} := (P(ab|xy)) \in \mathbb{R}^{m^2\Delta^2}$, which we will refer to as the

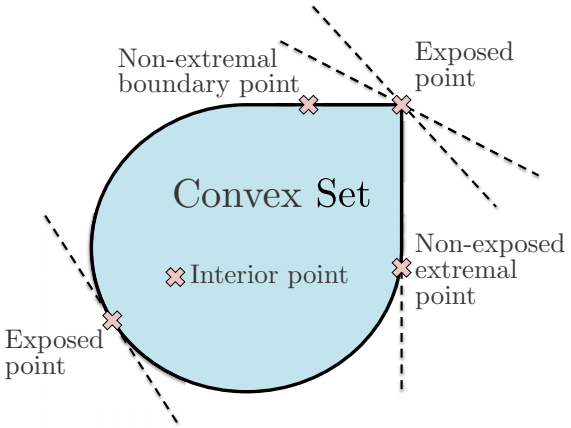

FIG. 1. Different types of points of a compact convex set.

behavior,[1] *probability point*, or simply a *point*. It is clear that all conditional probability distributions must be non-negative

$$P(ab|xy) \geqslant 0 \quad \forall a,b,x,y \tag{3}$$

and normalized

$$\sum_{ab} P(ab|xy) = 1 \quad \forall x,y. \tag{4}$$

1. The no-signaling set $\mathcal{NS}$

A probability point belongs to the no-signaling set if it satisfies

$$\begin{aligned} &\forall a,x,y,y' \ \sum_b P(ab|xy) = \sum_b P(ab|xy') \ \text{and} \\ &\forall b,x,x',y \ \sum_a P(ab|xy) = \sum_a P(ab|x'y)\,. \end{aligned} \tag{5}$$

The term *no-signaling* [38] refers to the fact that the choice of local settings of one party does not affect the outcome distribution of the other party. We denote the set of all no-signaling behaviors by $\mathcal{NS}$ and since it is characterized by a finite number of linear inequalities and equalities, namely (3), (4), and (5), the no-signaling set is a polytope.

2. The quantum set $\mathcal{Q}$

The quantum set $\mathcal{Q}$ is the set of correlations which can be achieved by performing local measurements on quantum systems. Following the standard tensor-product paradigm, each party is assigned a Hilbert space $\mathcal{H}$ of finite dimension $d := \dim(\mathcal{H}) < \infty$. A valid quantum state corresponds to a $d^2 \times d^2$ matrix which is positive semidefinite and of unit trace. A local measurement with Δ outcomes is a decomposition of the d-dimensional identity into positive semidefinite operators,

[1] Tsirelson first used the term "behavior" [10] to describe a family of probability distributions indexed by tuples of setting values. The term has become widely adopted, e.g., in Refs. [6,37]. The terms "box" [38,39], "probability model" [40], and "correlation" [41,42] are also commonly used.

i.e., $\{E_a\}_{a=1}^{\Delta}$ such that $E_a \geqslant 0$ for all a and

$$\sum_{a=1}^{\Delta} E_a = \mathbb{1}_d, \tag{6}$$

where $\mathbb{1}_d$ denotes the d-dimensional identity matrix.

We define $\mathcal{Q}_{\text{finite}}$ to be the set of behaviors which can be generated when local Hilbert spaces are finite-dimensional, i.e., $\vec{P} \in \mathcal{Q}_{\text{finite}}$ if there exists a finite-dimensional quantum state ρ and measurements $\{E_a^x\},\{F_b^y\}$ such that

$$P(ab|xy) = \text{tr}\left[\left(E_a^x \otimes F_b^y\right)\rho\right] \tag{7}$$

for all a,b,x,y.

To make the underlying mathematics neater, we define the quantum set $\mathcal{Q}$ as the closure of $\mathcal{Q}_{\text{finite}}$; i.e., we explicitly include all the limit points, which makes the quantum set $\mathcal{Q}$ compact.[2] The fundamental result that $\mathcal{Q} \neq \mathcal{Q}_{\text{finite}}$ for some finite Bell scenarios was only recently established by Slofstra [43] (see also the recent work of Dykema *et al.* [44]).

3. The local set $\mathcal{L}$

We call a probability point *deterministic* if the output of each party is a (deterministic) function of their input and we denote the set of deterministic points by $\mathcal{L}_{\text{det}}$. The local set is defined as the convex hull of the deterministic points

$$\mathcal{L} := \text{Conv}\,[\mathcal{L}_{\text{det}}].$$

Since $\mathcal{L}_{\text{det}}$ is a finite set, the local set $\mathcal{L}$ is a polytope.

B. Bell functions and exposed faces of the correlation sets

A *Bell function* is a real vector $\vec{B} \in \mathbb{R}^{m^2\Delta^2}$ and the value of the function on a specific behavior $\vec{P}$ is simply the inner product $\vec{B} \cdot \vec{P}$. For a given correlation set $\mathcal{S} = \mathcal{L},\mathcal{Q},\mathcal{NS}$ we denote the maximum value of the Bell function by

$$\beta_{\mathcal{S}}(\vec{B}) := \max_{\vec{P}\in\mathcal{S}} \vec{B} \cdot \vec{P}.$$

Note that since all these sets are compact, the maximum is always achieved. To simplify the notation, we will simply write $\beta_{\mathcal{S}}$ whenever the Bell function is clear from the context.

Bell functions are useful for studying the three correlation sets, but they suffer from the problem of nonuniqueness; i.e., the same function can be written in multiple ways which are not always easily recognized as equivalent (see, however, Ref. [45]). To overcome this obstacle, instead of studying the inequalities we study the (exposed) faces they give rise to. For a correlation set $\mathcal{S} = \mathcal{L},\mathcal{Q},\mathcal{NS}$, every Bell function $\vec{B}$ identifies a face

$$\mathcal{F}_{\mathcal{S}}(\vec{B}) := \{\vec{P} \in \mathcal{S} : \vec{B} \cdot \vec{P} = \beta_{\mathcal{S}}\}.$$

All the sets considered here are compact, so the face is always nonempty; i.e., it contains at least one point. Since the local set $\mathcal{L}$ and the no-signaling set $\mathcal{NS}$ are polytopes, all their faces are also guaranteed to be polytopes, while for the quantum set $\mathcal{Q}$ this is not necessarily the case.

The dimension of the face $\mathcal{F}_{\mathcal{S}}(\vec{B})$ is simply the dimension of the affine subspace spanned by the points in $\mathcal{F}_{\mathcal{S}}(\vec{B})$. While the dimensions of local and no-signaling faces are easy to compute (we simply find which vertices saturate the maximal value and then check how many of them are affinely independent), there is no generic way of computing the dimension of a quantum face. However, if the quantum value coincides with either the local or the no-signaling value, an appropriate bound follows directly from the set inclusion relation (1):

$$\beta_{\mathcal{Q}}(\vec{B}) = \beta_{\mathcal{L}}(\vec{B}) \Rightarrow \dim(\mathcal{F}_{\mathcal{Q}}(\vec{B})) \geqslant \dim(\mathcal{F}_{\mathcal{L}}(\vec{B})) \tag{8}$$

and

$$\beta_{\mathcal{Q}}(\vec{B}) = \beta_{\mathcal{NS}}(\vec{B}) \Rightarrow \dim(\mathcal{F}_{\mathcal{Q}}(\vec{B})) \leqslant \dim(\mathcal{F}_{\mathcal{NS}}(\vec{B})). \tag{9}$$

A *flat boundary region* is an exposed face which contains more than a single point which is strictly smaller than the entire set.[3]

Focusing on faces, rather than Bell functions, reduces the undesired ambiguity; the following example shows that multiple Bell functions may give rise to the same face. Let $\vec{P}$ be a deterministic point and recall that for such a point all the conditional probabilities are either zero or one. Consider a Bell function $\vec{B}$ whose coefficients satisfy

$$B(abxy)\begin{cases} >0 & \text{if } \; P(ab|xy) = 1, \\ =0 & \text{otherwise.} \end{cases} \tag{10}$$

Every Bell function in this (continuous) family has a unique maximizer, which is precisely the point $\vec{P}$ (regardless of the choice of the correlation set). This simple example illustrates that (i) multiple Bell functions can have precisely coinciding sets of maximizers (i.e., they give rise to the same face) and (ii) all deterministic probability points are exposed in all three sets $\mathcal{L},\mathcal{Q}$, and $\mathcal{NS}$ (see Appendix A for the definition of an exposed point).

Bell functions can be split into four (disjoint) classes by comparing the maximal values over the three correlation sets:

(1) $\beta_{\mathcal{L}} < \beta_{\mathcal{Q}} < \beta_{\mathcal{NS}}$: all three values differ,

(2) $\beta_{\mathcal{L}} = \beta_{\mathcal{Q}} < \beta_{\mathcal{NS}}$: only local and quantum values coincide,

(3) $\beta_{\mathcal{L}} < \beta_{\mathcal{Q}} = \beta_{\mathcal{NS}}$: only quantum and no-signaling values coincide,

(4) $\beta_{\mathcal{L}} = \beta_{\mathcal{Q}} = \beta_{\mathcal{NS}}$: all three values coincide.

Whenever two of these values coincide, we can make the classification finer by asking whether the resulting faces coincide or not. In the list below, we fine-grain the four Bell-value classes into nine face-comparison classes, using $=$ vs $\subsetneq$ to distinguish exact coincidence from strict containment. Enumerating all possible cases leads to

(1) $\beta_{\mathcal{L}} < \beta_{\mathcal{Q}} < \beta_{\mathcal{NS}}$,
(2a) $\beta_{\mathcal{L}} = \beta_{\mathcal{Q}} < \beta_{\mathcal{NS}}$ and $\mathcal{F}_{\mathcal{L}} \subsetneq \mathcal{F}_{\mathcal{Q}}$,
(2b) $\beta_{\mathcal{L}} = \beta_{\mathcal{Q}} < \beta_{\mathcal{NS}}$ and $\mathcal{F}_{\mathcal{L}} = \mathcal{F}_{\mathcal{Q}}$,
(3a) $\beta_{\mathcal{L}} < \beta_{\mathcal{Q}} = \beta_{\mathcal{NS}}$ and $\mathcal{F}_{\mathcal{Q}} \subsetneq \mathcal{F}_{\mathcal{NS}}$,
(*3b) $\beta_{\mathcal{L}} < \beta_{\mathcal{Q}} = \beta_{\mathcal{NS}}$ and $\mathcal{F}_{\mathcal{Q}} = \mathcal{F}_{\mathcal{NS}}$,
(4a) $\beta_{\mathcal{L}} = \beta_{\mathcal{Q}} = \beta_{\mathcal{NS}}$ and $\mathcal{F}_{\mathcal{L}} \subsetneq \mathcal{F}_{\mathcal{Q}} \subsetneq \mathcal{F}_{\mathcal{NS}}$,
(4b) $\beta_{\mathcal{L}} = \beta_{\mathcal{Q}} = \beta_{\mathcal{NS}}$ and $\mathcal{F}_{\mathcal{L}} = \mathcal{F}_{\mathcal{Q}} \subsetneq \mathcal{F}_{\mathcal{NS}}$,

[2] A detailed treatment of this issue, which is of secondary importance in the context of this work, can be found in Appendix B.

[3] One should take care not to confuse the face $\mathcal{F}_{\mathcal{S}}(\vec{B})$ with the hyperplane $\vec{B} \cdot \vec{P} = \beta_{\mathcal{S}}$: The face $\mathcal{F}_{\mathcal{S}}(\vec{B})$ is the intersection of $\mathcal{S}$ with the hyperplane.

(*4c) $\beta_{\mathcal{L}} = \beta_{\mathcal{Q}} = \beta_{\mathcal{NS}}$ and $\mathcal{F}_{\mathcal{L}} \subsetneq \mathcal{F}_{\mathcal{Q}} = \mathcal{F}_{\mathcal{NS}}$,
(4d) $\beta_{\mathcal{L}} = \beta_{\mathcal{Q}} = \beta_{\mathcal{NS}}$ and $\mathcal{F}_{\mathcal{L}} = \mathcal{F}_{\mathcal{Q}} = \mathcal{F}_{\mathcal{NS}}$.

It turns out that two (those marked with $*$) among these nine cases are actually *not* realizable. Indeed, no nonlocal vertex of the no-signaling polytope can be obtained by measuring quantum systems [46], which places some restrictions on the cases satisfying $\beta_{\mathcal{Q}} = \beta_{\mathcal{NS}}$. The face $\mathcal{F}_{\mathcal{NS}}$ is the convex hull of some vertices of the no-signaling polytope. If all these vertices are local, we must have $\mathcal{F}_{\mathcal{L}} = \mathcal{F}_{\mathcal{NS}}$, which puts us in the class (4d). On the other hand, if there is at least one nonlocal vertex, this vertex does not belong to the quantum set. This immediately implies that $\mathcal{F}_{\mathcal{Q}} \subsetneq \mathcal{F}_{\mathcal{NS}}$, which eliminates classes (3b) and (4c). All the remaining classes exist and some of them we discuss in detail, e.g., class (1) in Sec. III A, (2a) in Sec. III B 1, (2b) in Sec. III B 2 (see the generic cases considered therein), (4a) in Sec. G 2, and (4b) in Sec. III C 2. Class (3a) does not appear in the (2-2-2) scenario (see Appendix D for a proof), but it is easy to check that the magic square game [47] or the (tripartite) Mermin inequality [8] belong precisely to that class. Class (4d) is represented by the family of inequalities defined in Eq. (10) (although the resulting face is just a single point; a one-dimensional example of this kind is given in Appendix G 1).

C. Self-testing of quantum systems

Some probability points in the quantum set have the surprising property that there is essentially only one way of realizing them in quantum mechanics, a phenomenon known as *self-testing*. In this paper, we do not prove any new self-testing results, but we provide explicit examples where the usual self-testing statements cannot be made. Moreover, we prove a relation between self-testing and extremality (see Appendix C for details), which we use to deduce that certain points are extremal in the quantum set.

III. FACES OF THE QUANTUM SET IN THE (2-2-2) SCENARIO

In this paper, we focus predominantly on the simplest nontrivial Bell scenario, i.e., the case of $m = \Delta = 2$. It is well known [48] that in this scenario the local set is fully described by the positivity inequalities (3), no-signaling constraints (5), and eight additional inequalities, which are all equivalent (up to permutations of inputs and outputs) to the CHSH inequality [7]. The existence of a single type of (facet) Bell inequalities and the fact that any no-signaling probability point $\vec{P} \in \mathcal{NS}$ can violate at most one of these inequalities [49] means that we can interpret the CHSH violation as a measure of distance from the local set. More specifically, Bierhorst showed that the total variation distance from the local set and the local content [50] can be written as linear functions of the violation [51]. In Appendix E, we show that the same property holds for various notions of *visibility*.

The structure of the quantum set turns out to be significantly more complex. Let us start by introducing convenient notation for the (2-2-2) scenario. Correlations in the (2-2-2) scenario are described by vectors $\vec{P} \in \mathbb{R}^{16}$, but due to the no-signaling constraints these vectors span only an eight-dimensional subspace and it is convenient to use a representation which takes advantage of this dimension reduction. Following the convention $a,b \in \{0,1\}$ we define the local marginals as

$$\langle A_x \rangle := P(a=0|x) - P(a=1|x),$$
$$\langle B_y \rangle := P(b=0|y) - P(b=1|y)$$

and the correlators as

$$\langle A_x B_y \rangle := P(a=b|xy) - P(a \neq b|xy).$$

The inverse relation is given by

$$P(ab|xy) = \tfrac{1}{4}[1 + (-1)^a \langle A_x \rangle + (-1)^b \langle B_y \rangle + (-1)^{a+b} \langle A_x B_y \rangle]. \tag{11}$$

While this transformation is valid for any no-signaling point, the notation is inspired by quantum mechanics, since for a quantum behavior the local marginals and correlators are simply expectation values [$\langle X \rangle = \mathrm{tr}(X\rho)$] of the local observables

$$A_x = E_0^x - E_1^x,$$
$$B_y = F_0^y - F_1^y$$

and their products. The expectation values are conveniently represented in a table

$$\vec{P} = \begin{array}{c|c|c} & \langle B_0 \rangle & \langle B_1 \rangle \\ \hline \langle A_0 \rangle & \langle A_0 B_0 \rangle & \langle A_0 B_1 \rangle \\ \hline \langle A_1 \rangle & \langle A_1 B_0 \rangle & \langle A_1 B_1 \rangle \end{array} \tag{12}$$

and it is natural to use the same representation when writing down Bell functions. It is worth pointing out that the coordinate transformation that takes us from the conditional probabilities of events $P(ab|xy)$ to the local marginals $(\langle A_x \rangle, \langle B_y \rangle)$ and correlators $(\langle A_x B_y \rangle)$ is a linear transformation, but it is not isometric. In other words, the transformation does not change any qualitative features of the set, e.g., whether a point is extremal or exposed, but it might affect measures of distance or volume. In order to make this transformation isometric, we would need to define our coordinate system as $(c_1\langle A_x \rangle, c_1\langle B_y \rangle, c_2\langle A_x B_y \rangle)$ for suitably chosen constants c_1, c_2.

In the remainder of the section, we look at various quantum faces in the (2-2-2) scenario ordered according to the classification introduced in Sec. II B.

A. A quantum face with $\beta_{\mathcal{L}} < \beta_{\mathcal{Q}} < \beta_{\mathcal{NS}}$

Our first example is the CHSH Bell function [7], which reads

$$\vec{B}_1 := \begin{array}{c|c|c} & 0 & 0 \\ \hline 0 & 1 & 1 \\ \hline 0 & 1 & -1 \end{array}, \quad \vec{B}_1 \cdot \vec{P} \leqslant \begin{cases} 2 & \mathcal{L} \\ \mathbf{2\sqrt{2}} & \mathcal{Q} \\ 4 & \mathcal{NS} \end{cases}. \tag{13}$$

This function is known to have a unique quantum maximizer [6,52]

$$\vec{P}_{\mathrm{CHSH}} := \begin{array}{c|c|c} & 0 & 0 \\ \hline 0 & \frac{1}{\sqrt{2}} & \frac{1}{\sqrt{2}} \\ \hline 0 & \frac{1}{\sqrt{2}} & -\frac{1}{\sqrt{2}} \end{array}, \tag{14}$$

which implies that $\vec{P}_{\mathrm{CHSH}}$ is an exposed point of the quantum set. In Fig. 2, we show $\vec{P}_{\mathrm{CHSH}}$ in the two-dimensional

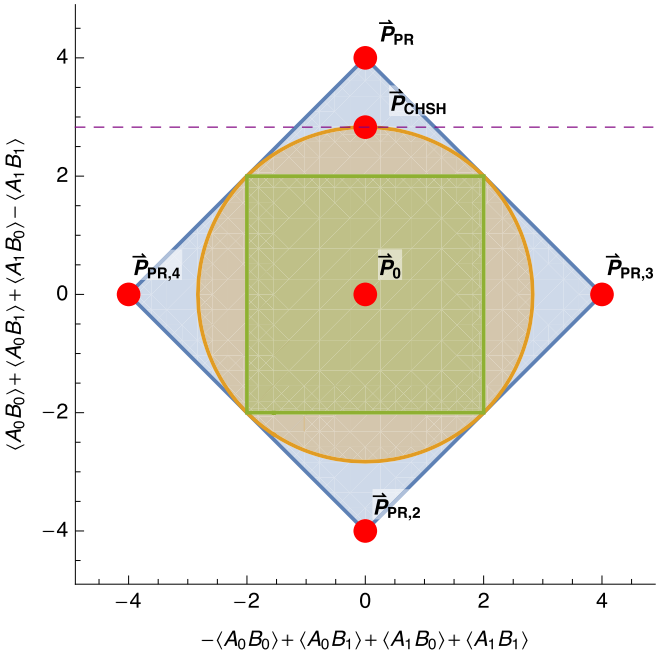

FIG. 2. A two-dimensional slice in which the quantum set exhibits no flat boundaries (first presented as Fig. 1 in Ref. [12]). Points on this slice can also be conveniently parametrized by two different versions of the CHSH Bell functions as in Fig. 3 of Ref. [21].

slice spanned by four variants of the Popescu-Rohrlich (PR) box [6,38,39,46,53]

$$\vec{P}_{\rm PR} := \begin{array}{c|cc} & 0 & 0 \\ \hline 0 & 1 & 1 \\ 0 & 1 & -1 \end{array}, \quad \vec{P}_{\rm PR,\,2} := \begin{array}{c|cc} & 0 & 0 \\ \hline 0 & -1 & -1 \\ 0 & -1 & 1 \end{array},$$
$$\vec{P}_{\rm PR,\,3} := \begin{array}{c|cc} & 0 & 0 \\ \hline 0 & -1 & 1 \\ 0 & 1 & 1 \end{array}, \quad \vec{P}_{\rm PR,\,4} := \begin{array}{c|cc} & 0 & 0 \\ \hline 0 & 1 & -1 \\ 0 & -1 & -1 \end{array}. \tag{15}$$

The central point of this plot corresponds to the uniformly random distribution, which can be written as a uniform mixture of the four PR boxes, i.e.,

$$\vec{P}_0 := \begin{array}{c|cc} & 0 & 0 \\ \hline 0 & 0 & 0 \\ 0 & 0 & 0 \end{array}. \tag{16}$$

B. Quantum faces with $\beta_{\mathcal{L}} = \beta_{\mathcal{Q}} < \beta_{\mathcal{NS}}$

In this section, we consider Bell functions satisfying $\beta_{\mathcal{L}} = \beta_{\mathcal{Q}}$, which implies that the corresponding quantum faces will contain some local points.

1. *Quantum faces with $\mathcal{F}_{\mathcal{L}} \subsetneq \mathcal{F}_{\mathcal{Q}}$ containing the CHSH point*

Consider the Bell function

$$\vec{B}_2 := \begin{array}{c|cc} & 1-\sqrt{2} & 1 \\ \hline 1-\sqrt{2} & \sqrt{2} & \sqrt{2} \\ 1 & \sqrt{2} & -\sqrt{2} \end{array}, \quad \vec{B}_2 \cdot \vec{P} \leqslant \begin{cases} 4 & \mathcal{L} \\ \mathbf{4} & \mathcal{Q} \\ 4\sqrt{2} & \mathcal{NS} \end{cases}, \tag{17}$$

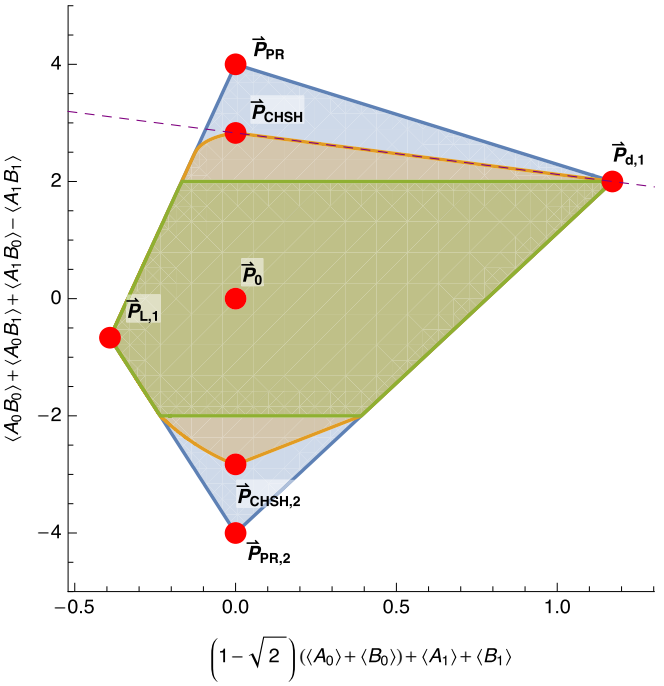

FIG. 3. A slice containing $\vec{P}_{\rm CHSH}$, $\vec{P}_0$, and $\vec{P}_{d,1}$ is singled out by the following six equations: $\langle A_0\rangle = \langle A_1\rangle = \langle B_0\rangle = \langle B_1\rangle$, $\langle A_0B_0\rangle = \langle A_0B_1\rangle = \langle A_1B_0\rangle$, and $\langle A_0\rangle + \langle A_1\rangle + \langle B_0\rangle + \langle B_1\rangle = 2(\langle A_0B_0\rangle + \langle A_1B_1\rangle)$. The point $\vec{P}_{L,1}$ is given by $\langle A_x\rangle = \langle B_y\rangle = \langle A_xB_y\rangle = -1/3$. Apart from the flat quantum face $\mathcal{F}_{\mathcal{Q}}(\vec{B}_2)$ that connects $\vec{P}_{\rm CHSH}$ and $\vec{P}_{d,1}$, our numerical results suggest a few other flat regions on the boundary of (this slice of) the quantum set.

where the local and no-signaling bounds have been computed by enumerating the vertices of the polytopes, while the quantum bound has been computed using the analytic technique of Wolfe and Yelin [54]. The quantum bound is saturated by $\vec{P}_{\rm CHSH}$ but also by the deterministic point

$$\vec{P}_{d,1} := \begin{array}{c|cc} & 1 & 1 \\ \hline 1 & 1 & 1 \\ 1 & 1 & 1 \end{array}. \tag{18}$$

This implies that the resulting quantum face is *at least* one-dimensional and we conjecture that this lower bound is actually tight, i.e., that the quantum face is a line. Figure 3 shows this quantum face in the slice containing $\vec{P}_{\rm CHSH}$, $\vec{P}_0$, and $\vec{P}_{d,1}$ (the same feature was presented in Fig. 3(c) of Ref. [36]).

The above quantum face is not the only flat face containing $\vec{P}_{\rm CHSH}$. To see this, we swap the outcomes of all the measurements: This results in flipping the horizontal axis of Fig. 3 while leaving the vertical axis unchanged. This relabelling transforms the Bell function $\vec{B}_2$ to

$$\vec{B}_{2^*} := \begin{array}{c|cc} & \sqrt{2}-1 & -1 \\ \hline \sqrt{2}-1 & \sqrt{2} & \sqrt{2} \\ -1 & \sqrt{2} & -\sqrt{2} \end{array}, \quad \vec{B}_{2^*} \cdot \vec{P} \leqslant \begin{cases} 4 & \mathcal{L} \\ \mathbf{4} & \mathcal{Q} \\ 4\sqrt{2} & \mathcal{NS} \end{cases},$$

whose quantum value is achieved by $\vec{P}_{\rm CHSH}$ and

$$\vec{P}_{d,2} := \begin{array}{c|cc} & -1 & -1 \\ \hline -1 & 1 & 1 \\ -1 & 1 & 1 \end{array}. \tag{19}$$

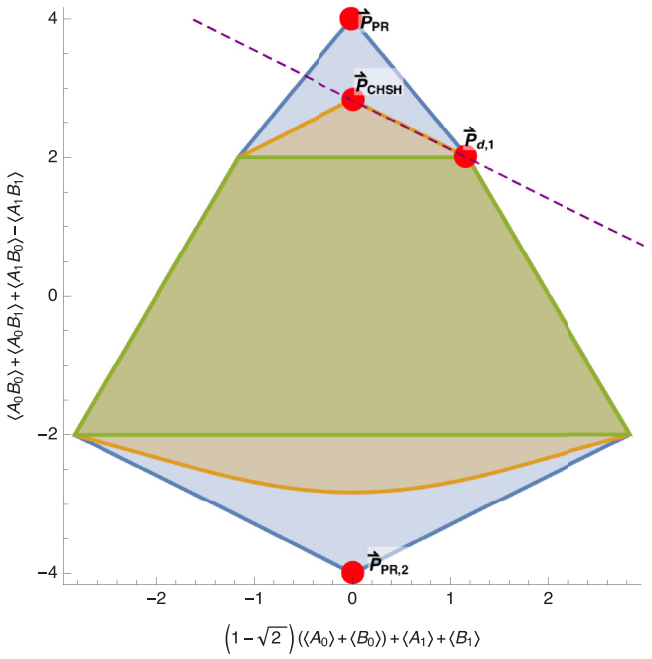

FIG. 4. Projection illustrating the flat boundary identified by $\vec{B}_1$. While every point in a slice plot corresponds to precisely one behavior, a point in a projection plot may simultaneously represent multiple behaviors. In this projection, the behaviors $\vec{P}_{\text{CHSH}}$ and $\vec{P}_{d,1}$ are the only behaviors that lie on the points $(0,2\sqrt{2})$ and $(4-2\sqrt{2},2)$, respectively. We see that all three correlation sets are symmetric with respect to the reflection about the $x=0$ line. This symmetry arises from the relabelling of the outcomes of all measurements, which flips the marginals but leaves the correlators unchanged.

This immediately implies that a *projection* plot of $\mathcal{Q}$ using the same set of axes must look different from the *slice* plot, a difference which is clearly seen in Figs. 3 and 4. More generally, we can apply a suitably chosen relabelling of the inputs and/or outputs to obtain an equivalent face that connects $\vec{P}_{\text{CHSH}}$ with any of the eight deterministic points which saturate the local value of the CHSH inequality given in Eq. (13).

It is worth pointing out that the *nonextremal* probability points lying on these quantum faces *cannot* be obtained by performing measurements on two-qubit states. In other words, only the $\vec{P}_{\text{CHSH}}$ and the corresponding local deterministic point are quantumly achievable using local Hilbert spaces of dimension 2—as can be verified using the technique of Ref. [36], Appendix D. Aside from this example, there are many more additional faces of the quantum set which contain a deterministic point and an extremal nonlocal point. For a systematic method of finding them, please refer to Appendix F.

2. *Higher-dimensional quantum faces with $\mathcal{F}_{\mathcal{L}} \subsetneq \mathcal{F}_{\mathcal{Q}}$*

Interestingly, higher-dimensional quantum faces containing nonlocal points can also be found in this simplest Bell scenario. Consider, for example, the following two-parameter family of Bell functions:

$$\vec{B}_3 := \begin{array}{c|c|c} & -a & 1 \\ \hline -a & c & c \\ \hline 1 & c & -(c+1-2a) \end{array},$$

$$\vec{B}_3 \cdot \vec{P} \leqslant \begin{cases} 2c+1 & \mathcal{L} \\ \mathbf{2c+1} & \mathcal{Q} \\ 4c+1-2a & \mathcal{NS} \end{cases}, \tag{20}$$

where $a \in [0,1]$ and $c \in [a, c_{\max}]$ with $c_{\max}$ being—for any given value of a—the largest value of c for which the following inequality holds:

$$(c-2a+1)[2a^3-3a^2+(3a-1)c^2-5(a-1)ac-c^3]$$
$$\geqslant \frac{a^2}{4c^2}[-2a^2+3(a-1)c+a+c^2]^2. \tag{21}$$

The quantum bound of Eq. (20) is saturated by three deterministic points: $\vec{P}_{d,1}$ given in Eq. (18) and

$$\vec{P}_{d,3} := \begin{array}{c|c|c} & -1 & 1 \\ \hline -1 & 1 & -1 \\ \hline -1 & 1 & -1 \end{array}, \quad \vec{P}_{d,4} := \begin{array}{c|c|c} & -1 & -1 \\ \hline -1 & 1 & 1 \\ \hline 1 & -1 & -1 \end{array}. \tag{22}$$

Note that $\vec{P}_{d,3}$ and $\vec{P}_{d,4}$ are related by simply swapping Alice and Bob, i.e., transposing the matrix given in Eq. (22).

Interestingly, for generic pairs (a,c), the quantum inequality is saturated *exclusively* by local points. On the other hand, when we consider special pairs of (a,c) at the limit of the region constrained by Eq. (21), we find that the quantum bound is saturated by an additional extremal nonlocal point. Table I lists several functions from this *one-parameter* family together with some properties of the extremal nonlocal maximizers.

For nonmaximal values of c, we have $\mathcal{F}_{\mathcal{L}} = \mathcal{F}_{\mathcal{Q}}$, whereas for maximal c the quantum face extends into an additional dimension beyond the local subspace, i.e., $\mathcal{F}_{\mathcal{L}} \subsetneq \mathcal{F}_{\mathcal{Q}}$. The increase in the dimension can be easily seen by noting that all three local points saturating Eq. (20) give the CHSH value of 2, which is exceeded by the additional quantum point. As we further increase a, we reach the values $a=c=1$, which corresponds to a linear combination of positivity facets.

C. Bell functions with $\beta_{\mathcal{L}} = \beta_{\mathcal{Q}} = \beta_{\mathcal{NS}}$

In Sec. II B, we have already seen a family of Bell functions with $\beta_{\mathcal{L}} = \beta_{\mathcal{Q}} = \beta_{\mathcal{NS}}$ for which the resulting faces are identical, $\mathcal{F}_{\mathcal{L}} = \mathcal{F}_{\mathcal{Q}} = \mathcal{F}_{\mathcal{NS}}$. In this section, we present examples of the remaining two classes.

1. *A Bell function satisfying $\mathcal{F}_{\mathcal{L}} \subsetneq \mathcal{F}_{\mathcal{Q}} \subsetneq \mathcal{F}_{\mathcal{NS}}$ containing an extremal but nonexposed point*

Consider the Bell function

$$\vec{B}_4 := \begin{array}{c|c|c} & 0 & 0 \\ \hline 0 & 0 & 0 \\ \hline 0 & 0 & -1 \end{array}, \quad \vec{B}_4 \cdot \vec{P} \leqslant \begin{cases} 1 & \mathcal{L} \\ \mathbf{1} & \mathcal{Q} \\ 1 & \mathcal{NS} \end{cases}.$$

We do not have an analytic characterization of the corresponding quantum face, but we can show that it is not a polytope. More specifically, we show that already in the slice of unbiased marginals $\langle A_0\rangle = \langle A_1\rangle = \langle B_0\rangle = \langle B_1\rangle = 0$ the quantum face has an infinite number of extremal points. The analytic characterization of the quantum set in the correlator space due to Tsirelson, Landau, and Masanes [10,25,55] states that correlators $\langle A_x B_y\rangle$ belong to the quantum set if and only

TABLE I. Each row corresponds to a Bell function from the family defined in Eq. (20). The parameters a and c, chosen to saturate Eq. (21), determine the quantum bound $\beta_{\mathcal{Q}}$ of the function. The quantum face identified by each function consists of (at least) four extremal points: three deterministic points and one nonlocal point. The remaining three columns contain information about the nonlocal maximizer: the CHSH violation β_{CHSH}, the entanglement of the optimal two-qubit state λ (quantified by the square of the larger Schmidt coefficient, e.g., $\lambda = 1/2$ corresponds to the maximally entangled state), and the optimal angle ϕ between the two local observables ($\phi = 90^\circ$ corresponds to maximally incompatible observables). The optimal angle is always the same for both parties, which reflects the symmetry of the Bell function. The final row corresponds to a Bell function saturated exclusively by local points; i.e., there is no nonlocal maximizer. It is interesting to examine the trends in the properties of the nonlocal maximizer. The maximally entangled state appears only for $a = \frac{\sqrt{17}-3}{4} \approx 0.280776$, with the entanglement of the state dropping monotonically as a varies away from that special value in either direction. The angle between the observables decreases monotonically as a increases while maximal incompatibility is observed for $a = \frac{1}{3}(14\sqrt{13}\sin z - 23)$, where $z := \frac{1}{6}[\pi - 2\tan^{-1}(87\sqrt{3}/4591)]$; i.e., $a \approx 0.586417$. Finally, the CHSH violation initially increases and then goes down, peaking at $\beta_{\mathrm{CHSH}} \approx 2.810$ for $a \approx 0.45$.

a	c	$\beta_{\mathcal{Q}}$	β_{CHSH}	λ	ϕ
0.1	0.325	1.649	2.719	0.558	106.945°
0.2	0.592	2.185	2.769	0.525	103.131°
0.280776	0.781	2.562	2.792	**0.5**	100.358°
0.5	1.193	3.386	2.808	0.564	93.091°
0.586417	1.318	3.635	2.798	0.591	**90°**
0.6	1.335	3.670	2.795	0.596	89.486°
0.7	1.444	3.889	2.766	0.631	85.336°
0.8	1.510	4.020	2.711	0.674	80.075°
0.846074	1.519	4.038	2.671	0.699	76.924°
0.9	1.502	4.004	2.599	0.737	72.036°
0.99	1.272	3.543	2.249	0.878	50.291°
1	1	3	n/a	n/a	n/a

if

$$1 + \prod_{xy}\langle A_x B_y\rangle + \prod_{xy}\sqrt{1-\langle A_x B_y\rangle^2} - \frac{1}{2}\sum_{xy}\langle A_x B_y\rangle^2 \geqslant 0, \tag{23}$$

where the sums and products go over $x, y \in \{0,1\}$.[4] The quantum set in the correlator space is a *projection* of the (full) quantum set onto the coordinates $(\langle A_0B_0\rangle, \langle A_0B_1\rangle, \langle A_1B_0\rangle, \langle A_1B_1\rangle)$. However, since all such correlations can be achieved with unbiased marginals [56], the possible values of correlators in the slice of unbiased marginals are described precisely by constraint (23). The quantum face is characterized by $\langle A_1B_1\rangle = -1$, which leads to a cubic inequality

$$2\langle A_0B_0\rangle\langle A_0B_1\rangle\langle A_1B_0\rangle + \langle A_0B_0\rangle^2 + \langle A_0B_1\rangle^2 + \langle A_1B_0\rangle^2 \leqslant 1.$$

[4]This elegant and symmetric form is obtained by simply squaring the inequality derived by Landau [25].

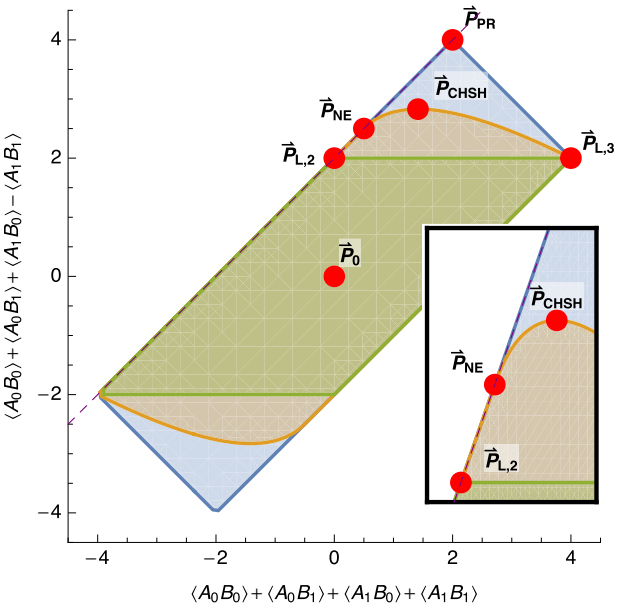

FIG. 5. A highly symmetric two-dimensional slice of the quantum set. Thanks to the analytic characterization of the quantum set given in Eq. (24), we can rigorously show that $\vec{P}_{\mathrm{NE}}$ is a nonexposed point of the quantum set.

Any point which saturates this inequality and additionally satisfies

$$\max\{|\langle A_0B_0\rangle|, |\langle A_0B_1\rangle|, |\langle A_1B_0\rangle|\} < 1$$

is a self-test [57] and, hence, must be an extremal point of the quantum set (see Appendix C for a proof). It is easy to verify that there is an infinite number of such points and, therefore, the quantum face corresponding to the Bell function $\vec{B}_4$ must have an infinite number of extremal points.

The strict inclusions $\mathcal{F}_{\mathcal{L}} \subsetneq \mathcal{F}_{\mathcal{Q}} \subsetneq \mathcal{F}_{\mathcal{NS}}$ are intuitively clear and neatly presented in a particular slice. In Fig. 5, we present a two-dimensional slice containing the PR box $\vec{P}_{\mathrm{PR}}$ and two local behaviors

$$\vec{P}_{L,2} = \begin{array}{c|c|c} & 0 & 0 \\ \hline 0 & 1/3 & 1/3 \\ \hline 0 & 1/3 & -1 \end{array} \quad \text{and} \quad \vec{P}_{L,3} = \begin{array}{c|c|c} & 0 & 0 \\ \hline 0 & 1 & 1 \\ \hline 0 & 1 & 1 \end{array}.$$

This slice is singled out by unbiased marginals and three of the correlators being equal $\langle A_0B_0\rangle = \langle A_0B_1\rangle = \langle A_1B_0\rangle$. Points in this slice are conveniently parametrized by $\langle A_1B_1\rangle$ and

$$\alpha = \langle A_0B_0\rangle = \langle A_0B_1\rangle = \langle A_1B_0\rangle.$$

The constraint given in Eq. (23) implies the following tight upper bound on $(-\langle A_1B_1\rangle)$ as a function of α:

$$-\langle A_1B_1\rangle \leqslant \begin{cases} 1 & -1 \leqslant \alpha < 1/2 \\ 3\alpha - 4\alpha^3 & 1/2 \leqslant \alpha \leqslant 1 \end{cases}. \tag{24}$$

Let us consider the point at the boundary which corresponds to $\alpha = 1/2$, i.e.,

$$\vec{P}_{\mathrm{NE}} = \begin{array}{c|c|c} & 0 & 0 \\ \hline 0 & 1/2 & 1/2 \\ \hline 0 & 1/2 & -1 \end{array}. \tag{25}$$

This is precisely where the flat and curved parts of the boundary meet and it is easy to check that the gradients on both sides are equal, which implies that the point $\vec{P}_{\mathrm{NE}}$ is not exposed in this slice. Since an exposed point must remain exposed in every slice, we conclude that $\vec{P}_{\mathrm{NE}}$ is not exposed in the entire set. However, we know that $\vec{P}_{\mathrm{NE}}$ is an extremal point, because it is a self-test [57]. We conjecture that any probability point which (i) saturates the constraint (23) and (ii) has precisely one correlator of unit modulus is of this type, i.e., extremal but not exposed.

It turns out that similar geometric features are exhibited by the so-called Hardy point, i.e., the (unique) point that maximally violates the Hardy paradox [35]. The Hardy point is a self-test [58] and therefore extremal, but it is not exposed (see Appendix H for a proof). This explains why previous attempts to find a Bell function that fully captures the nonlocal nature of the Hardy paradox failed. The authors of Ref. [59] proposed a sequence of Bell functions, whose maximizer approaches the Hardy point, but when one tries to take the limit, the coefficients of the functions diverge. This is precisely the behavior one would expect when dealing with an extremal but not exposed point. A family of quantum faces that the Hardy point lies on is discussed in Appendix G 2.

2. *A quantum face with $\mathcal{F}_{\mathcal{L}} = \mathcal{F}_{\mathcal{Q}} \subsetneq \mathcal{F}_{\mathcal{NS}}$*

Let us finish the discussion of the (2-2-2) scenario with an example of a quantum face which completely coincides with its local counterpart but is strictly contained within the no-signaling face. Consider the Bell function

$$\vec{B}_5 := \begin{array}{c|c|c} & 0 & 0 \\ \hline 0 & 1 & 1 \\ \hline 0 & 0 & 0 \end{array}, \quad \vec{B}_5 \cdot \vec{P} \leqslant \begin{cases} 2 & \mathcal{L} \\ \mathbf{2} & \mathcal{Q} \\ 2 & \mathcal{NS} \end{cases}. \tag{26}$$

We start by determining the quantum face $\mathcal{F}_{\mathcal{Q}}$. The maximal quantum value is achieved if and only if (iff) $\langle A_0 B_0\rangle = \langle A_0 B_1\rangle = 1$, which by constraint (23) implies that $\langle A_1 B_0\rangle = \langle A_1 B_1\rangle$. It is, however, straightforward to verify that such correlations are local (they cannot violate any variant of the CHSH inequality) and thus $\mathcal{F}_{\mathcal{L}} = \mathcal{F}_{\mathcal{Q}}$. On the other hand, the PR box also saturates the bound given in Eq. (26), thus showing that $\mathcal{F}_{\mathcal{L}} = \mathcal{F}_{\mathcal{Q}} \subsetneq \mathcal{F}_{\mathcal{NS}}$.

IV. NONLOCAL FACES OF POSITIVE DIMENSION

Our numerical studies of the quantum set in the (2-2-2) scenario suggest that every Bell function for which $\beta_{\mathcal{Q}} > \beta_{\mathcal{L}}$ has a unique maximizer in the quantum set. While we conjecture that this is indeed true in the (2-2-2) scenario, it is easy to see that it does not hold in general; e.g., if we take the CHSH inequality and "embed" it in a Bell scenario with more inputs, then the maximal violation does not carry any information about the statistics corresponding to the additional inputs. A more natural family of such functions was proposed by Slofstra [60], but these require a large number of measurement settings on each side. On the other hand, a simple example was recently found in the tripartite (3-2-2) scenario by Ramanathan and Mironowicz [61]. In this section, we give an example in the bipartite scenario (2-3-2) and two additional examples in the (3-2-2) scenario. What is particularly appealing about the tripartite examples is that we were able to fully determine the corresponding quantum faces.

A. The (2-3-2) scenario

Consider the correlation part of the I_{3322} Bell function [62,63]

$$\begin{aligned}\vec{B}_6 \cdot \vec{P} := {} & \langle A_0 B_0\rangle + \langle A_0 B_1\rangle + \langle A_0 B_2\rangle + \langle A_1 B_0\rangle \\ & + \langle A_1 B_1\rangle - \langle A_1 B_2\rangle + \langle A_2 B_0\rangle - \langle A_2 B_1\rangle. \end{aligned} \tag{27}$$

The local and no-signaling values of this inequality have been found by enumerating the vertices of the respective polytopes, whereas the quantum value has been found using a semidefinite program [64] (see Appendix I for details):

$$\vec{B}_6 \cdot \vec{P} \leqslant \begin{cases} 4 & \mathcal{L} \\ \mathbf{5} & \mathcal{Q} \\ 8 & \mathcal{NS} \end{cases}. \tag{28}$$

Below we present a one-parameter family of quantum realizations which saturate the quantum bound of this Bell function. The shared state is $|\Psi_-\rangle = \frac{1}{\sqrt{2}}(|01\rangle - |10\rangle)$ and the observables are

$$\begin{aligned} A_0 &= \frac{1}{2}\Big(2\cos\frac{\pi}{6}\,\sigma_x + \cos\alpha\,\sigma_y + \sin\alpha\,\sigma_z\Big), \\ A_1 &= \frac{1}{2}\Big(2\cos\frac{\pi}{6}\,\sigma_x - \cos\alpha\,\sigma_y - \sin\alpha\,\sigma_z\Big), \\ A_2 &= \sigma_y, \\ B_0 &= -\cos\frac{\pi}{6}\,\sigma_x - \sin\frac{\pi}{6}\,\sigma_y, \\ B_1 &= -\cos\frac{\pi}{6}\,\sigma_x + \sin\frac{\pi}{6}\,\sigma_y, \\ B_2 &= -\cos\alpha\,\sigma_y - \sin\alpha\,\sigma_z, \end{aligned}$$

where $\alpha \in [0, 2\pi]$ is a free parameter. It is clear that all the marginals vanish, $\langle A_x\rangle = \langle B_y\rangle = 0$, while the correlators are given by

$$\begin{aligned} \langle A_0 B_0\rangle = \langle A_1 B_1\rangle &= \frac{3+\cos\alpha}{4}, \\ \langle A_0 B_1\rangle = \langle A_1 B_0\rangle &= \frac{3-\cos\alpha}{4}, \\ \langle A_0 B_2\rangle = \langle A_2 B_0\rangle &= \frac{1}{2}, \\ \langle A_1 B_2\rangle = \langle A_2 B_1\rangle &= -\frac{1}{2}, \\ \langle A_2 B_2\rangle &= \cos\alpha. \end{aligned}$$

This family of probability points is simply a line whose extremal points correspond to $\alpha = 0$ and $\alpha = \pi$. Moreover, it is easy to check that the two extremal points are related by swapping A_0 with A_1 and flipping the sign of B_2 (since the Bell function is symmetric we could alternatively swap B_0 and B_1 and flip the sign of A_2).

We do not know whether the quantum face corresponding to $\vec{B}_6$ is strictly larger than the line, but the existence of such a one-dimensional region already has interesting implications for self-testing. More concretely, it means that saturating the quantum bound $\beta_{\mathcal{Q}} = 5$ does not imply the usual self-testing statement, simply because the maximal value can be achieved

by multiple inequivalent arrangements of observables.[5] It is, however, still possible that saturating the quantum bound certifies the maximally entangled state of two qubits. If so, this would be an example where the maximal violation certifies the state but not the measurements.

B. The tripartite scenarios

Finally, we discuss two tripartite examples which demonstrate that the geometry of the quantum set becomes even more complex in the multipartite scenarios.

The quantum set for multiple parties has been extensively studied, but mainly in the context of Bell inequalities. From the study of multipartite self-testing, we know that certain Bell functions have unique maximizers, e.g., the Bell function proposed by Mermin [68] (and its generalization due to Mermin, Ardehali, Belinskii and Klyshko [67]), but also the Bell functions constructed to self-test the W state [69]. However, we conjecture that this behavior is not generic and present two Bell functions in the tripartite scenario which give rise to more complex quantum faces. In contrast to the bipartite scenario discussed before, in these cases we can explicitly map out the entire quantum face. The multiple inequivalent ways of saturating the quantum bound immediately imply specific limitations on the self-testing statements we can hope for.

In both examples, Alice, Bob, and Charlie perform binary measurements. In the first example, Alice and Bob have two measurements, whereas Charlie only has one. Consider the Bell function

$$\vec{B}_7 \cdot \vec{P} := \langle A_0 B_0 C_0\rangle + \langle A_0 B_1 C_0\rangle + \langle A_1 B_0 C_0\rangle - \langle A_1 B_1 C_0\rangle,$$

which first appeared as Eq. (15) in Ref. [26]. Note that this is nothing else than the CHSH function between Alice and Bob "modulated" by the outcome of Charlie, which immediately implies that $\beta_{\mathcal{L}} = 2, \beta_{\mathcal{Q}} = 2\sqrt{2}$ and $\beta_{\mathcal{NS}} = 4$. The quantum bound is saturated when Alice and Bob perform the optimal CHSH strategy while Charlie deterministically outputs 0, which leads to[6]

$$\begin{aligned} \langle A_x\rangle = \langle B_y\rangle = 0,\ \langle C_0\rangle = 1,\\ \langle A_x B_y\rangle = \langle A_x B_y C_0\rangle = (-1)^{xy}/\sqrt{2},\\ \langle A_x C_0\rangle = \langle B_y C_0\rangle = 0. \end{aligned} \tag{29}$$

Alternatively, the quantum bound may be saturated if Alice and Bob achieve the CHSH value of $-2\sqrt{2}$, while Charlie deterministically outputs 1, which leads to

$$\begin{aligned} \langle A_x\rangle = \langle B_y\rangle = 0,\ \langle C_0\rangle = -1,\\ -\langle A_x B_y\rangle = \langle A_x B_y C_0\rangle = (-1)^{xy}/\sqrt{2},\\ \langle A_x C_0\rangle = \langle B_y C_0\rangle = 0. \end{aligned} \tag{30}$$

Since Charlie always performs the same measurement, for the purpose of computing the resulting statistics we can assume that he is only classically correlated with Alice and Bob. Conditioned on a particular output of Charlie, the statistics on Alice and Bob are unique, as they must achieve the CHSH value of $+2\sqrt{2}$ or $-2\sqrt{2}$. This implies that we always end up with a convex combinations of statistics given in Eqs. (29) and (30), i.e., that the resulting quantum face is simply a line.

Any point on this line can be realized using a three-qubit state shared among Alice, Bob, and Charlie. In fact, it suffices to look at a single arrangement of qubit observables

$$\begin{aligned} &A_0 = \sigma_x, && A_1 = \sigma_z,\\ &B_0 = (\sigma_x + \sigma_z)/\sqrt{2}, && B_1 = (\sigma_x - \sigma_z)/\sqrt{2},\\ &C_0 = \sigma_z. \end{aligned} \tag{31}$$

The largest eigenvalue of the resulting Bell operator equals $\lambda = 2\sqrt{2}$ and the corresponding eigenspace is two-dimensional and spanned by vectors $\{|\Phi_+\rangle_{AB}|0\rangle_C, |\Psi_-\rangle_{AB}|1\rangle_C\}$, where $|\Phi_+\rangle = (|00\rangle + |11\rangle)/\sqrt{2}$ and $|\Psi_-\rangle = (|01\rangle - |10\rangle)/\sqrt{2}$. Therefore, the quantum bound is saturated by any state of the form

$$|\eta\rangle_{ABC} := \cos\theta\, |\Phi_+\rangle_{AB}|0\rangle_C + \sin\theta\, |\Psi_-\rangle_{AB}|1\rangle_C$$

for $\theta \in [0,\pi/2]$. In fact, since Charlie always measures in the computational basis, the same statistics could be obtained from the mixed state[7]

$$\begin{aligned} \rho_{ABC} = \cos^2\theta\, |\Phi_+\rangle\langle\Phi_+|_{AB} \otimes |0\rangle\langle 0|_C\\ + \sin^2\theta\, |\Psi_-\rangle\langle\Psi_-|_{AB} \otimes |1\rangle\langle 1|_C, \end{aligned}$$

which clearly results in a convex combination of the two extremal points.

It is instructive to consider what kind of self-testing statements we can hope for in this case. Grouping Bob and Charlie brings us back to the CHSH scenario (in the sense that Bob and Charlie together have only two distinct measurement settings), so there must be a maximally entangled two-qubit state in the bipartition Alice vs Bob and Charlie, but we do not know exactly how the entanglement is split between Bob and Charlie. At the extremal points given by Eqs. (29) and (30), the reduced statistics on Alice and Bob saturate the quantum bound of some CHSH function, which ensures that the relevant entanglement is shared between Alice and Bob only. In the interior of the line, however, we cannot make such precise statements. In particular, while all the interior points can be realized using genuinely tripartite entanglement, such entanglement can never be certified in this setup, simply because the entire line can be written as a convex combination

[5] In most cases of self-testing, it is sufficient to allow for extra degrees of freedom and local isometries (see Appendix C for details), but sometimes one must also consider the transposition (complex conjugation) equivalence [65,66]. The transposition equivalence is automatically taken care of if one looks at commutation relations between the local observables [67], which immediately implies that the quantum realizations presented in the main text are inequivalent even if we allow for this additional equivalence.

[6] It is well known that in a tripartite scenario with two outcomes per site the probability point is uniquely determined by the local marginals and the two- and three-body expectation values; see, e.g., Ref. [70].

[7] The same mixed state was recently used by Krisnanda *et al.* to demonstrate that quantum systems can become entangled even if they interact only through a mediator which remains classical (diagonal in a fixed basis) at all times [71].

of the extremal points (which can be achieved using bipartite entanglement between Alice and Bob).

In the second example, there are two measurements on each site; i.e., we are in the (3-2-2) scenario. Consider the Bell function

$$\vec{B}_8 \cdot \vec{P} := \langle A_0B_0C_0\rangle + \langle A_0B_1C_1\rangle + \langle A_1B_0C_0\rangle - \langle A_1B_1C_1\rangle$$

for which $\beta_{\mathcal{L}} = 2, \beta_{\mathcal{Q}} = 2\sqrt{2}$ and $\beta_{\mathcal{NS}} = 4$. This Bell function was found by Werner and Wolf while characterizing the facets of the correlation polytope in the (3-2-2) scenario [26], but as shown in Ref. [72] it is also a facet Bell inequality of the full local polytope. We show in Appendix J that the corresponding quantum face is the convex hull of eight discrete points and a one-parameter family of quantum points arising from the tripartite Greenberger-Horne-Zeilinger (GHZ) state [73].

The eight points, denoted by $\{\vec{P}_j\}_{j=1}^8$, are achieved when Alice saturates some variant of the CHSH function with either Bob or Charlie, while the remaining party adopts a deterministic strategy. The one-parameter family corresponds to Bob and Charlie nontrivially "sharing" the maximal CHSH violation.

The first two points correspond to Charlie always producing the same outcome regardless of his input. The resulting statistics are analogous to those in Eqs. (29) and (30):

$$\begin{aligned} &\langle A_x\rangle = \langle B_y\rangle = 0,\ \langle C_z\rangle = 1,\\ \vec{P}_1:\quad &\langle A_xB_y\rangle = \langle A_xB_yC_z\rangle = (-1)^{xy}/\sqrt{2},\\ &\langle A_xC_z\rangle = \langle B_yC_z\rangle = 0, \end{aligned}$$

and

$$\begin{aligned} &\langle A_x\rangle = \langle B_y\rangle = 0,\ \langle C_z\rangle = -1,\\ \vec{P}_2:\quad &-\langle A_xB_y\rangle = \langle A_xB_yC_z\rangle = (-1)^{xy}/\sqrt{2},\\ &\langle A_xC_z\rangle = \langle B_yC_z\rangle = 0. \end{aligned}$$

Points $\vec{P}_3$ and $\vec{P}_4$ arise if Charlie's outcome depends on his input, which implies that Alice and Bob must saturate another variant of the CHSH inequality. The resulting statistics are

$$\begin{aligned} &\langle A_x\rangle = \langle B_y\rangle = 0,\\ &\langle C_0\rangle = 1,\ \langle C_1\rangle = -1,\\ \vec{P}_3:\quad &\langle A_xB_y\rangle = (-1)^{(x+1)y}/\sqrt{2},\\ &\langle A_xB_yC_z\rangle = (-1)^{(x+1)y+z}/\sqrt{2},\\ &\langle A_xC_z\rangle = \langle B_yC_z\rangle = 0, \end{aligned}$$

and

$$\begin{aligned} &\langle A_x\rangle = \langle B_y\rangle = 0,\\ &\langle C_0\rangle = -1,\ \langle C_1\rangle = 1,\\ \vec{P}_4:\quad &\langle A_xB_y\rangle = (-1)^{(x+1)y+1}/\sqrt{2},\\ &\langle A_xB_yC_z\rangle = (-1)^{(x+1)y+z}/\sqrt{2},\\ &\langle A_xC_z\rangle = \langle B_yC_z\rangle = 0. \end{aligned}$$

Points $\{P_j\}_{j=5}^8$ are constructed from $\{P_j\}_{j=1}^4$ by exchanging the roles of Bob and Charlie.

The one-parameter family of facial points has vanishing one- and two-body expectation values

$$\langle A_x\rangle = \langle B_y\rangle = \langle C_z\rangle = \langle A_xB_y\rangle = \langle A_xC_z\rangle = \langle B_yC_z\rangle = 0,$$

while the three-body correlations are given by

$$\begin{aligned} \langle A_0B_0C_0\rangle &= \langle A_0B_1C_1\rangle = \frac{1}{\sqrt{2}},\\ \langle A_0B_0C_1\rangle &= \langle A_0B_1C_0\rangle = \cos\alpha,\\ \langle A_1B_0C_0\rangle &= -\langle A_1B_1C_1\rangle = \frac{1}{\sqrt{2}},\\ \langle A_1B_0C_1\rangle &= -\langle A_1B_1C_0\rangle = \sin\alpha \end{aligned} \tag{32}$$

for $\alpha \in [0, 2\pi]$.

This example is important because we can explicitly compute the corresponding quantum face and we see that it is a highly nontrivial object. We conjecture that in multipartite scenarios such high-dimensional and nonpolytopic quantum faces are a common phenomenon.

V. CONCLUSIONS AND OPEN QUESTIONS

In this work, we have studied the geometry of the quantum set. In particular, we have identified several flat regions lying on the boundary of the quantum set and we have found extremal points which are not exposed. We have also introduced a classification of Bell functions in terms of the facial structure they give rise to and provided an explicit example for each existing class. Finally, we have presented a simple example of a bipartite Bell function whose quantum and classical values differ for which the quantum maximizer is not unique.

Despite the progress we have made on understanding the geometry of the quantum set in the (2-2-2) scenario, several questions remain open. For instance, having found a one-dimensional flat boundary region containing the CHSH point, one could ask whether it is possible to find a higher dimensional region of that kind or, more generally, what is the highest dimension of a flat region containing the CHSH point. Let us also put forward the following conjecture about the uniqueness of the maximizer: From our numerics it seems that all Bell functions in the (2-2-2) scenario have at most one extremal nonlocal maximizer. Can one find an analytical proof of this statement?

Another interesting task would be to study the extremal points of the quantum set in the (2-2-2) scenario. We know that all of them can be achieved by projective measurements on a two-qubit state, but we know that the latter is a strict superset of the former. This is particularly interesting from the self-testing point of view: We know that if the marginals are uniform, then all the extremal nonlocal points are self-tests. Is this also true for correlation points with arbitrary marginals? In other words, are all extremal nonlocal points of the quantum set in the (2-2-2) scenario self-tests?

Another natural question arising from our results concerns the "generic" geometry of the quantum set. In this work, we provide several examples of unexpected geometric features of the quantum set, but in order to see them one has to go beyond the standard, well-studied Bell functions. Therefore, the question is whether such features are indeed "unusual"

or our intuition has simply been skewed by looking only at "regular" Bell functions for which these behaviors do not appear. We suspect that such features are indeed unusual, but we currently have no rigorous evidence to support this claim.

ACKNOWLEDGMENTS

We would like to thank Eliahu Cohen for showing us the elegant form of the Tsirelson-Landau-Masanes criterion, Laura Mančinska for bringing to our attention Ref. [46], and Denis Rosset and Antonios Varvitsiotis for useful discussions. This research is supported by the Singapore Ministry of Education Academic Research Fund Tier 3 (Grant No. MOE2012-T3-1-009), the National Research Fund and the Ministry of Education, Singapore, under the Research Centres of Excellence programme, the John Templeton Foundation project "Many-box locality as a physical principle" (Grant No. 60607), the European Union's Horizon 2020 research and innovation programme under the Marie Skłodowska-Curie Action ROSETTA (Grant No. 749316), the European Research Council (Grant No. 337603), the Danish Council for Independent Research (Sapere Aude), the VILLUM FONDEN via the QMATH Centre of Excellence (Grant No. 10059), the National Research, Development, and Innovation Office NKFIH (Grants No. K111734 and No. KH125096), the Ministry of Education of Taiwan, R.O.C., through "Aiming for the Top University Project" granted to the National Cheng Kung University (NCKU), the Ministry of Science and Technology of Taiwan, R.O.C. (Grant No. 104-2112-M-006-021-MY3), and in part by Perimeter Institute for Theoretical Physics. Research at Perimeter Institute is supported by the Government of Canada through the Department of Innovation, Science, and Economic Development Canada and by the Province of Ontario through the Ministry of Research, Innovation, and Science.

APPENDIX A: CONVEX SETS

In this appendix, we introduce standard notions and definitions used in convex geometry. For more details, we refer the reader to Chapters 1 and 8 of Ref. [74].

Let $\mathcal{A}$ be a convex subset of $\mathbb{R}^d$ and, moreover, suppose that $\mathcal{A}$ is compact (i.e., closed and bounded). For an arbitrary vector $\vec{g} \in \mathbb{R}^d$ let

$$c(\vec{g}) := \max_{\vec{u}\in\mathcal{A}} \vec{g}\cdot\vec{u}$$

and note that the hyperplane $\{\vec{u} \in \mathbb{R}^d : \vec{u}\cdot\vec{g} = c(\vec{g})\}$ is a *supporting hyperplane*; i.e., it has a nonempty intersection with $\mathcal{A}$ and it divides the space into two half-spaces such that $\mathcal{A}$ is fully contained in one of them. The vector $\vec{g}$ represents a linear functional acting on $\mathbb{R}^d$. It is well known that every convex set can be described as an intersection of half-spaces (possibly infinite). Supporting hyperplanes help us to understand the boundary of the convex set. For an arbitrary functional $\vec{g}$, the set of points which maximize $\vec{g}$

$$\mathcal{F}(\vec{g}) := \{\vec{u} \in \mathcal{A} : \vec{g}\cdot\vec{u} = c(\vec{g})\}$$

is called an *exposed face* of $\mathcal{A}$ and since $\mathcal{A}$ is compact, the face is always nonempty. An exposed face is called *proper* if $\mathcal{F}(\vec{g}) \subsetneq \mathcal{A}$.

A point $\vec{u} \in \mathcal{A}$ is called a *boundary point* if it belongs to some proper exposed face and we denote the set of boundary points by $\mathcal{A}_{\text{bnd}}$. The set of interior points of $\mathcal{A}$ is simply the complement of $\mathcal{A}_{\text{bnd}}$ (in $\mathcal{A}$).

Some boundary points have the property that they cannot be written as a nontrivial convex combination of other points in the set. Such points are called *extremal* and we denote the set of extremal points by $\mathcal{A}_{\text{ext}}$. The Krein-Milman theorem states that any convex compact set (in a finite-dimensional vector space) is equal to the convex hull of its extremal points

$$\mathcal{A} = \text{Conv}(\mathcal{A}_{\text{ext}}).$$

Therefore, when maximizing a linear functional over the set, it suffices to perform the optimization over its extremal points. In other words, for all $\vec{g}$ we have

$$\max_{\vec{g}\in\mathcal{A}} \vec{g}\cdot\vec{u} = \max_{\vec{g}\in\mathcal{A}_{\text{ext}}} \vec{g}\cdot\vec{u}.$$

Knowing the extremal points of $\mathcal{A}$ is also sufficient to determine its faces. Since a face is a convex compact set, it is equal to the convex hull of its extremal points and the extremal points of the face must also be extremal points of $\mathcal{A}$. For exposed faces, we have

$$\mathcal{F}(\vec{g}) = \text{Conv}(\{\vec{u} \in \mathcal{A}_{\text{ext}} : \vec{g}\cdot\vec{u} = c(\vec{g})\}).$$

Among extremal points, there are points which can be identified as *unique* maximizers of some linear functional. We say that $\vec{u}$ is *exposed* if there exists a linear functional $\vec{g}$ such that

$$\mathcal{F}(\vec{g}) = \{\vec{u}\}$$

and we denote the set of exposed points by $\mathcal{A}_{\text{exp}}$. From the definitions alone, we immediately establish the inclusions

$$\mathcal{A}_{\text{exp}} \subseteq \mathcal{A}_{\text{ext}} \subseteq \mathcal{A}_{\text{bnd}} \subseteq \mathcal{A}$$

and it is well known that all of them are in general strict. However, it is worth pointing out that by Straszewicz's theorem in a finite-dimensional vector space the set of exposed points is dense in the set of extremal points (Ref. [75], Theorem 3). In other words, extremal but nonexposed points should be regarded as exceptional. For a polytope, the set of extremal and exposed points coincide, as they are simply the vertices of the polytope.

APPENDIX B: PRECISE DEFINITION OF THE QUANTUM SET

Here we give a precise definition of the quantum set using the notions introduced in Sec. II A 2 (quantum state and local quantum measurements). We also show why the description becomes significantly simpler in any (n-2-2) scenario.

Let $\mathcal{Q}_d$ be the set of all probability points which can be realized using systems of local dimension d. Since both the set of states and the set of measurements of fixed (local) dimension are compact and the trace is a continuous map, all these sets are closed; i.e., for all $d \in \mathbb{N}$ we have

$$\text{Clos}(\mathcal{Q}_d) = \mathcal{Q}_d.$$

We then define the set $\mathcal{Q}_{\text{finite}}$ as the infinite union

$$\mathcal{Q}_{\text{finite}} := \bigcup_{d\in\mathbb{N}} \mathcal{Q}_d$$

and the quantum set $\mathcal{Q}$ as the closure

$$\mathcal{Q} := \text{Clos}(\mathcal{Q}_{\text{finite}}).$$

While $\mathcal{Q}_d$ is not necessarily convex, the union $\mathcal{Q}_{\text{finite}}$ is and so is the quantum set $\mathcal{Q}$. Since $\mathcal{Q}$ is bounded (all the components of the probability vector must belong to the interval $[0,1]$) and closed (by definition), it is a compact set.

While in general we might have to consider quantum systems of arbitrary large dimensions, Jordan's lemma simplifies the problem in the (n-2-2) scenario. Jordan's lemma states that any two (Hermitian) projectors P and Q can be simultaneously block diagonalized such that the blocks are of size at most 2×2 [27]. This implies that in any scenario with two binary measurements on each site for any $d\in\mathbb{N}$ we have

$$\mathcal{Q}_d \subseteq \text{Conv}(\mathcal{Q}_2),$$

which immediately implies

$$\mathcal{Q}_{\text{finite}} \subseteq \text{Conv}(\mathcal{Q}_2).$$

If we start with the inclusion relation

$$\mathcal{Q}_2 \subseteq \mathcal{Q}_{\text{finite}} \subseteq \text{Conv}(\mathcal{Q}_2)$$

and take convex hulls recalling that $\text{Conv}(\mathcal{Q}_{\text{finite}}) = \mathcal{Q}_{\text{finite}}$, we arrive at

$$\mathcal{Q}_{\text{finite}} = \text{Conv}(\mathcal{Q}_2).$$

Since $\mathcal{Q}_2$ is closed and the convex hull of a closed set is still closed, we finally obtain

$$\mathcal{Q} = \text{Conv}(\mathcal{Q}_2).$$

Let us mention that this observation (for the special case of $n=2$) was already made by Tsirelson in 1980 [56].

APPENDIX C: SELF-TESTING OF QUANTUM SYSTEMS

In this appendix, we give a formal definition of self-testing and prove a relation between self-testing and extremality.

Let $\vec{P}\in\mathcal{Q}_{\text{finite}}$ be a quantum probability point. A quantum realization of $\vec{P}$ consists of Hilbert spaces $\mathcal{H}_A$ and $\mathcal{H}_B$, a state ρ_{AB} acting on $\mathcal{H}_A\otimes\mathcal{H}_B$ and local measurements $\{E_a^x\}$ and $\{F_b^y\}$ acting on $\mathcal{H}_A$ and $\mathcal{H}_B$, respectively, such that

$$P(ab|xy) = \text{tr}\left[\left(E_a^x\otimes F_b^y\right)\rho_{AB}\right]$$

for all a,b,x,y. We denote this quantum realization by $(\mathcal{H}_A,\mathcal{H}_B,\rho_{AB},\{E_a^x\},\{F_b^y\})$.

It turns out that for certain quantum probability points all quantum realizations are closely related. This is conveniently formulated by finding a single realization from which all other realizations can be generated and we will call such a realization *canonical*. In the standard formulation of self-testing, one can never certify that the state is mixed or that the measurements are nonprojective (every point in the quantum set can be obtained by performing projective measurements on a pure state). Therefore, the canonical realization always consists of projective measurements acting on a pure state. Moreover, we embed it in local Hilbert spaces whose dimension is equal to the rank of the reduced state, which ensures that the reduced density matrices are full rank. We denote the canonical realization by $(\mathcal{H}_{A'},\mathcal{H}_{B'},\Psi_{A'B'},\{P_a^x\},\{Q_b^y\})$. We use the standard definition of self-testing (see, e.g., Ref. [52]), but we formulate it at the level of density matrices.

Definition C.1. A quantum probability point $\vec{P}\in\mathcal{Q}_{\text{finite}}$ self-tests the canonical quantum realization $(\mathcal{H}_{A'},\mathcal{H}_{B'},\Psi_{A'B'},\{P_a^x\},\{Q_b^y\})$ if for every realization of $\vec{P}$, denoted by $(\mathcal{H}_A,\mathcal{H}_B,\rho_{AB},\{E_a^x\},\{F_b^y\})$, we can find

(1) Hilbert spaces $\mathcal{H}_{A''}$ and $\mathcal{H}_{B''}$,

(2) local isometries

$$V_A : \mathcal{H}_A \to \mathcal{H}_{A'}\otimes\mathcal{H}_{A''},$$
$$V_B : \mathcal{H}_B \to \mathcal{H}_{B'}\otimes\mathcal{H}_{B''},$$

(3) an auxiliary quantum state $\sigma_{A''B''}$ acting on $\mathcal{H}_{A''}\otimes\mathcal{H}_{B''}$ such that for $V := V_A\otimes V_B$ we have

$$V\left[\left(E_a^x\otimes F_b^y\right)\rho_{AB}\right]V^\dagger = \left[\left(P_a^x\otimes Q_b^y\right)\Psi_{A'B'}\right]\otimes\sigma_{A''B''} \quad \text{(C1)}$$

for all a,b,x,y.

This equality ensures that applying the real measurement operators to the real state is equivalent to applying the ideal measurements to the ideal state. Moreover, summing over a and b (for any fixed x and y) immediately gives

$$V\rho_{AB}V^\dagger = \Psi_{A'B'}\otimes\sigma_{A''B''}, \quad \text{(C2)}$$

which means that by applying local isometries one can find the ideal state $\Psi_{A'B'}$ inside the real state ρ_{AB}.

Let us start with the following simple observation.

Observation C.1. Let R_{GH}^0, R_{GH}^1 be positive semidefinite operators acting on $\mathcal{H}_G\otimes\mathcal{H}_H$ such that

$$R_{GH}^0 + R_{GH}^1 = S_G\otimes T_H, \quad \text{(C3)}$$

where S_G and T_H are positive semidefinite operators acting on $\mathcal{H}_G$ and $\mathcal{H}_H$, respectively. If $\text{rank}(S_G)=1$, then the operators R_{GH}^0 and R_{GH}^1 must be of the form

$$R_{GH}^j = S_G\otimes T_H^j$$

for some positive semidefinite T_H^j acting on $\mathcal{H}_H$.

Proof. If $\text{tr}(T_H)=0$, we must have $T_H=0$, which immediately implies $R_{GH}^j=0$; i.e., we can set $T_H^j=0$. If $\text{tr}(T_H)>0$, tracing out H in Eq. (C3) implies that $R_G^j=\alpha_j S_G$ for some $\alpha_j\geqslant 0$. It is easy to check that a bipartite positive semidefinite operator whose marginal is proportional to a rank-1 projector must be a product operator. ■

Now, we are ready to state and prove the main result of this appendix.

Proposition C.1. If a quantum probability point $\vec{P}\in\mathcal{Q}_{\text{finite}}$ self-tests the canonical realization $(\mathcal{H}_{A'},\mathcal{H}_{B'},\Psi_{A'B'},\{P_a^x\},\{Q_b^y\})$, then it must be an extremal point of $\mathcal{Q}_{\text{finite}}$.

Proof. We show that $\vec{P}$ cannot be written as a nontrivial convex combination of points in $\mathcal{Q}_{\text{finite}}$. More specifically, we show that if $\vec{P}$ is a self-test and can be written as

$$\vec{P} = q_0\vec{P}_0 + q_1\vec{P}_1 \quad \text{(C4)}$$

for $q_0,q_1\in(0,1), q_0+q_1=1$ and $\vec{P}_0,\vec{P}_1\in\mathcal{Q}_{\text{finite}}$, then we must necessarily have $\vec{P}_0=\vec{P}_1=\vec{P}$.

Since $\vec{P}_j \in \mathcal{Q}_{\text{finite}}$, it has a finite-dimensional realization on $\mathcal{H}_{A_j}$ and $\mathcal{H}_{B_j}$ given by

$$\left(\mathcal{H}_{A_j},\mathcal{H}_{B_j},\rho^j_{A_jB_j},\{E^{x,j}_a\},\{F^{y,j}_b\}\right)$$

and we choose a realization in which the reduced states are full rank, i.e., $\text{rank}(\rho_{A_j}) = \dim(\mathcal{H}_{A_j})$ and $\text{rank}(\rho_{B_j}) = \dim(\mathcal{H}_{B_j})$. Clearly, the convex combination given in Eq. (C4) can be realized on $\mathcal{H}_A := \mathcal{H}_{A_0} \oplus \mathcal{H}_{A_1}$ and $\mathcal{H}_B := \mathcal{H}_{B_0} \oplus \mathcal{H}_{B_1}$. Writing out $\mathcal{H}_A \otimes \mathcal{H}_B$ as a direct sum gives

$$\begin{aligned}\mathcal{H}_A \otimes \mathcal{H}_B &= (\mathcal{H}_{A_0} \oplus \mathcal{H}_{A_1}) \otimes (\mathcal{H}_{B_0} \oplus \mathcal{H}_{B_1}) \\ &= \mathcal{H}_{A_0B_0} \oplus \mathcal{H}_{A_0B_1} \oplus \mathcal{H}_{A_1B_0} \oplus \mathcal{H}_{A_1B_1}.\end{aligned}$$

We embed $\rho^0_{A_0B_0}$ and $\rho^1_{A_1B_1}$ as

$$\begin{aligned}\rho^0_{AB} &:= \rho^0_{A_0B_0} \oplus 0_{A_0B_1} \oplus 0_{A_1B_0} \oplus 0_{A_1B_1}, \\ \rho^1_{AB} &:= 0_{A_0B_0} \oplus 0_{A_0B_1} \oplus 0_{A_1B_0} \oplus \rho^1_{A_1B_1}\end{aligned}$$

and the overall state is given by

$$\rho_{AB} := q_0\rho^0_{AB} + q_1\rho^1_{AB}.$$

The measurement operators are given by

$$\begin{aligned}E^x_a &:= \left(E^{x,0}_a\right)_{A_0} \oplus \left(E^{x,1}_a\right)_{A_1}, \\ F^y_b &:= \left(F^{y,0}_b\right)_{B_0} \oplus \left(F^{y,1}_b\right)_{B_1}.\end{aligned}$$

Since $(\mathcal{H}_A,\mathcal{H}_B,\rho_{AB},\{E^x_a\},\{F^y_b\})$ is a quantum realization of $\vec{P}$ and $\vec{P}$ self-tests the canonical realization $(\mathcal{H}_{A'},\mathcal{H}_{B'},\Psi_{A'B'},\{P^x_a\},\{Q^y_b\})$, there exist Hilbert spaces $\mathcal{H}_{A''},\mathcal{H}_{B''}$, local isometries

$$\begin{aligned}V_A &: \mathcal{H}_A \to \mathcal{H}_{A'} \otimes \mathcal{H}_{A''}, \\ V_B &: \mathcal{H}_B \to \mathcal{H}_{B'} \otimes \mathcal{H}_{B''},\end{aligned}$$

and an auxiliary state $\sigma_{A''B''}$ such that

$$V\rho_{AB}V^\dagger = \Psi_{A'B'} \otimes \sigma_{A''B''},$$

where $V = V_A \otimes V_B$ is the combined isometry. If we write out the sum

$$q_0V\rho^0_{AB}V^\dagger + q_1V\rho^1_{AB}V^\dagger = \Psi_{A'B'} \otimes \sigma_{A''B''}, \tag{C5}$$

we obtain an equality to which Observation C.1 can be applied. To see that all the conditions are satisfied, we identify

$$\begin{aligned}\mathcal{H}_{A'} \otimes \mathcal{H}_{B'} &\leftrightarrow \mathcal{H}_G, \\ \mathcal{H}_{A''} \otimes \mathcal{H}_{B''} &\leftrightarrow \mathcal{H}_H, \\ q_jV\rho^j_{AB}V^\dagger &\leftrightarrow R^j_{GH}, \\ \Psi_{A'B'} &\leftrightarrow S_G, \\ \sigma_{A''B''} &\leftrightarrow T_H,\end{aligned}$$

which allows us to conclude that

$$q_jV\rho^j_{AB}V^\dagger = \Psi_{A'B'} \otimes q_j\sigma^j_{A''B''} \tag{C6}$$

for some normalized states $\sigma^j_{A''B''}$. Tracing out Bob's part of the state and dividing through by q_j (recall that $q_j > 0$) leads to

$$V_A\rho^j_AV^\dagger_A = \Psi_{A'} \otimes \sigma^j_{A''}. \tag{C7}$$

Since the quantum realizations of $\vec{P}_1$ and $\vec{P}_2$ and the canonical realization are locally full rank, the projectors on the supports of the reduced states are given by

$$\begin{aligned}\rho^0_A &\to \mathbb{1}_{A_0} \oplus 0_{A_1}, \\ \rho^1_A &\to 0_{A_0} \oplus \mathbb{1}_{A_1}, \\ \Psi_{A'} &\to \mathbb{1}_{A'}.\end{aligned}$$

Equation (C7) implies that the supports of both sides coincide, i.e.,

$$\begin{aligned}\Pi^0_A &:= V_A\left(\mathbb{1}_{A_0} \oplus 0_{A_1}\right)V^\dagger_A = \mathbb{1}_{A'} \otimes \Pi^0_{A''}, \\ \Pi^1_A &:= V_A\left(0_{A_0} \oplus \mathbb{1}_{A_1}\right)V^\dagger_A = \mathbb{1}_{A'} \otimes \Pi^1_{A''},\end{aligned}$$

where $\Pi^j_{A''}$ is the projector on the support of $\sigma^j_{A''}$. Similarly, for Bob we obtain

$$\begin{aligned}\Pi^0_B &:= V_B\left(\mathbb{1}_{B_0} \oplus 0_{B_1}\right)V^\dagger_B = \mathbb{1}_{B'} \otimes \Pi^0_{B''}, \\ \Pi^1_B &:= V_B\left(0_{B_0} \oplus \mathbb{1}_{B_1}\right)V^\dagger_B = \mathbb{1}_{B'} \otimes \Pi^1_{B''}.\end{aligned}$$

By applying the projector $\Pi^j_A \otimes \Pi^j_B$ to both sides of Eq. (C5) and taking the trace, we obtain

$$q_j = \text{tr}\left[\left(\Pi^j_{A''} \otimes \Pi^j_{B''}\right)\sigma_{A''B''}\right].$$

The self-testing condition (C1) states that

$$V\left[\left(E^x_a \otimes F^y_b\right)\rho_{AB}\right]V^\dagger = \left[\left(P^x_a \otimes Q^y_b\right)\Psi_{A'B'}\right] \otimes \sigma_{A''B''}.$$

Applying the projector $\Pi^j_A \otimes \Pi^j_B$ to both sides and tracing out gives

$$\begin{aligned}&q_j\,\text{tr}\left[\left(E^x_a \otimes F^y_b\right)\rho^j_{AB}\right] \\ &\quad= \text{tr}\left[\left(P^x_a \otimes Q^y_b\right)\Psi_{A'B'}\right]\text{tr}\left[\left(\Pi^j_{A''} \otimes \Pi^j_{B''}\right)\sigma_{A''B''}\right] \\ &\quad= q_j\,\text{tr}\left[\left(P^x_a \otimes Q^y_b\right)\Psi_{A'B'}\right],\end{aligned}$$

which immediately implies that $\vec{P}_j = \vec{P}$. ■

Since in the (2-2-2) scenario we have $\mathcal{Q} = \mathcal{Q}_{\text{finite}}$, this result is sufficient for our purposes. To prove a stronger result in which extremality in $\mathcal{Q}_{\text{finite}}$ is replaced by extremality in $\mathcal{Q}$, one needs a slightly stronger promise, namely that the self-testing property is *robust* (i.e., that all probability points lying sufficiently close to $\vec{P}$ "approximately" self-test the canonical realization). We leave this more general statement as an open problem for future work.

APPENDIX D: CLASS (3A) DOES NOT APPEAR IN THE (2-2-2) SCENARIO

We show here that in the (2-2-2) scenario the equality $\beta_\mathcal{Q} = \beta_{\mathcal{NS}}$ implies $\beta_\mathcal{L} = \beta_\mathcal{Q} = \beta_{\mathcal{NS}}$. Note that a similar result has been proven in a more general scenario (binary outcomes but an arbitrary number of settings), but for a special family of Bell functions (see Theorem 5.12 of Ref. [47]).

For an arbitrary Bell function, consider the vertices of the no-signaling polytope which saturate the no-signaling bound $\beta_{\mathcal{NS}}$. If any one of them is local, we immediately have $\beta_\mathcal{L} = \beta_{\mathcal{NS}}$, so we can without loss of generality assume that they are all nonlocal. If the bound is saturated by a single nonlocal vertex, then the quantum bound must be strictly smaller $\beta_\mathcal{Q} < \beta_{\mathcal{NS}}$, because the PR box lies outside of the quantum set. On

the other hand, if the bound is saturated by two (or more) nonlocal vertices, we must have $\beta_{\mathcal{L}} = \beta_{\mathcal{NS}}$. This is because in the (2-2-2) scenario the convex hull of any two nonlocal vertices of the no-signaling set always contains a local point (in fact, it suffices to mix the two vertices with equal weights).

APPENDIX E: THE CHSH VIOLATION VS DISTANCE MEASURES

In this appendix, we show that in the CHSH scenario various visibilities are simple functions of the CHSH violation β. It is known that any no-signaling point in the CHSH scenario can violate at most one CHSH inequality (see the last paragraph of the supplementary material of Ref. [49]), so the violation is well defined.

Since the local set is invariant under the relabelling of inputs and outputs, we can without loss of generality assume that it is the standard CHSH inequality, cf. Eq. (13), that is violated. Our results rely crucially on the following result proved by Bierhorst [51].

Proposition E.1. Let $\vec{P} \in \mathcal{NS}$ be a no-signaling point which violates the CHSH inequality, i.e., $\beta > 2$. Then $\vec{P}$ can be written as

$$\vec{P} = v_0 \vec{P}_{\text{PR}} + \sum_{j=1}^{8} v_j \vec{P}_j, \tag{E1}$$

where $v_j \geqslant 0$, $\sum_j v_j = 1$, and $\vec{P}_j$ correspond to the eight deterministic points which give the CHSH value of 2. Moreover, $v_0 = (\beta - 2)/2$.

For a no-signaling behavior, we define the *visibility* against noise coming from the set $\mathcal{S}$ as

$$v_{\mathcal{S}}(\vec{P}) := \inf\{\lambda \in [0,1] : (1-\lambda)\vec{P} + \lambda \vec{P}_{\text{noise}} \in \mathcal{L}\},$$

where $\vec{P}_{\text{noise}} \in \mathcal{S}$. The three cases of interest are (i) visibility against white noise $\mathcal{S} = \{\vec{P}_0\}$, (ii) visibility against local noise $\mathcal{S} = \mathcal{L}$, and (iii) visibility against no-signaling noise $\mathcal{S} = \mathcal{NS}$ and the results are

$$\begin{aligned} v_{\{\vec{P}_0\}}(\vec{P}) &= \frac{\beta - 2}{\beta}, \\ v_{\mathcal{L}}(\vec{P}) &= \frac{\beta - 2}{\beta + 2}, \\ v_{\mathcal{NS}}(\vec{P}) &= \frac{\beta - 2}{\beta + 4}. \end{aligned} \tag{E2}$$

These relations follow almost immediately from Proposition E.1. Writing $\vec{P}$ in the convex decomposition (E1) and adding noise leads to

$$(1-\lambda)v_0 \vec{P}_{\text{PR}} + (1-\lambda)\sum_{j=1}^{8} v_j \vec{P}_j + \lambda \vec{P}_{\text{noise}}.$$

Requiring that the CHSH value of the resulting point does not exceed the classical value of 2 is equivalent to

$$\lambda(\beta - \zeta) \geqslant \beta - 2,$$

where ζ is the CHSH value of $\vec{P}_{\text{noise}}$. As the right-hand side is strictly positive, we must have $\beta - \zeta > 0$, which allows us to rewrite this lower bound as

$$\lambda \geqslant \frac{\beta - 2}{\beta - \zeta}.$$

For white, local, and no-signaling noise, we have $\zeta = 0$, $\zeta \geqslant -2$ and $\zeta \geqslant -4$, respectively, thereby showing that the right-hand side of Eq. (E2) is a legitimate lower bound on the visibilities. To see that this amount of noise is also sufficient, choose $\vec{P}_{\text{noise}} = \vec{P}_0$, $\vec{P}_{\text{noise}} = (\vec{P}_0 + \vec{P}_{\text{PR},2})/2$, and $\vec{P}_{\text{noise}} = \vec{P}_{\text{PR},2}$, respectively.

The fact that the CHSH violation can be interpreted as a measure of distance from the local set might be useful in guiding us toward finding new robust self-tests. Suppose we would like to find a Bell inequality which self-tests a specific partially entangled state of two-qubits in the (2-2-2) scenario. Intuitively, we would like the probability point saturating this inequality to lie as far as possible from the local set. This reduces the problem to finding the maximal CHSH violation achievable using the fixed two-qubit state. It is worth pointing out that the self-tests for partially entangled two-qubit states based on the tilted CHSH inequality [76,77] satisfy this property.

APPENDIX F: IDENTIFYING AND CERTIFYING FLAT BOUNDARY REGIONS

To the best of our knowledge, the only rigorous method to certify the presence of a flat region on the boundary of the quantum set is to find a Bell function whose quantum value is saturated by distinct probability points. Since finding the quantum value of a Bell function is a well-studied problem, let us focus solely on the problem of identifying the relevant Bell function.

We are not aware of any systematic method of finding flat boundary regions of the quantum set. Instead, one has to start with some guesses and in our case they are predominantly of two types:

(i) Two Bell functions: we are given two Bell functions and we suspect that their maximal quantum values saturate some linear tradeoff.

(ii) A set of points: we are given a set of points and we suspect that they all lie on the same quantum face.

In the next two sections, we discuss how to handle cases (i) and (ii), respectively.

1. Making a projection plot

We are given two Bell functions $\vec{B}_1$ and $\vec{B}_2$ and we suspect that they saturate a linear tradeoff. To confirm this, we should produce a projection plot (similar to Fig. 4) and check for flat boundary regions. There is no exact method of performing such a projection, but we can compute an outer approximation using the Navascués-Pironio-Acín hierarchy and an inner approximation by providing explicit quantum realizations. Finding good inner approximations is particularly feasible in any (n-2-2) scenario, since we know that all extremal points of the quantum set can be achieved by performing projective measurements on an n-qubit state. We use the fact that projecting a convex compact set is equivalent to projecting

its extremal points and then taking the convex hull.[8] For instance, in the (2-2-2) scenario, we can fix the Schmidt basis to be the computational basis, i.e., assume that the bipartite state is of the form $|\psi\rangle = \cos\theta\,|00\rangle + \sin\theta\,|11\rangle$ for some $\theta \in [0,\pi/4]$. A rank-1 projective observable corresponds to a unit vector on the Bloch sphere, which is specified by two independent parameters. For two observables on each side this, gives nine parameters in total. Therefore, to generate the inner approximation of the projected quantum set, we must solve a series of nonlinear optimization problems in nine real variables. Such optimization problems can be solved numerically using standard numerical packages, but we are never guaranteed to converge to the global optimum. However, we have found that repeating the optimization with random starting points usually yields the correct answer.

Having identified a projection which contains a flat line on the boundary, we should look at its extremal points and find probability distributions that project down to these points. These need not be unique, but it suffices to find one for each of the endpoints. It is easy to see that a line connecting these two probability distributions lies on the boundary of the quantum set.

2. Finding the Bell function

Let $\{\vec{P}_j\}_j$ be the points which we suspect belong to the same quantum face. We are looking for a Bell function $\vec{B}$ whose quantum value is saturated by the points $\{\vec{P}_j\}_j$; i.e., we require that for all j

$$\vec{B}\cdot\vec{P}_j = 1 \tag{F1}$$

and $\beta_{\mathcal{Q}}(\vec{B}) = 1$.

The most primitive approach is to generate candidate Bell functions satisfying constraints (F1) and compute their quantum value. The tool used for computing the quantum value should ideally yield an analytic expression, as one can never distinguish between flat and almost-flat regions using numerical values. If all probability points exhibit a certain symmetry, we might also impose that symmetry on $\vec{B}$.

This method can be refined by looking at the neighborhood of the given probability points. Given a quantum realization of $\vec{P}_1$ it is easy to find some neighboring quantum points (e.g., applying rotations to the observables and/or the state). In the limit of infinitesimal change, this will give us a family of tangent vectors V_k such that $P_1 + \delta V_k \in \mathcal{Q}$ for sufficiently small δ. Clearly, we must have

$$\vec{B}\cdot\vec{V}_k = 0, \tag{F2}$$

which can significantly reduce the search space.

APPENDIX G: ADDITIONAL EXAMPLES OF QUANTUM FACES

1. A Bell function with $\mathcal{F}_{\mathcal{L}} = \mathcal{F}_{\mathcal{Q}} = \mathcal{F}_{\mathcal{NS}}$

We give here another example of a Bell function whose local, quantum, and no-signaling faces coincide, but in contrast to the examples given in Eq. (10) the maximizer is not unique. Consider the Bell function

$$\vec{B}_7 := \begin{array}{c|c|c} & 0 & 0 \\ \hline 0 & 1 & 1 \\ \hline 0 & 1 & 1 \end{array}, \quad \vec{B}_7\cdot\vec{P} \leqslant \begin{cases} 4 & \mathcal{L} \\ \mathbf{4} & \mathcal{Q} \\ 4 & \mathcal{NS} \end{cases}.$$

It is straightforward to verify that the only extremal no-signaling points which saturate this inequality are $\vec{P}_{d,1}$ and $\vec{P}_{d,2}$ [specified in Eqs. (18) and (19), respectively], i.e., that the resulting face is a line. Since both of these points are local, we immediately deduce that $\mathcal{F}_{\mathcal{L}} = \mathcal{F}_{\mathcal{Q}} = \mathcal{F}_{\mathcal{NS}}$.

2. Quantum faces containing the Hardy point

Let us start by presenting a quantum face of maximal dimension. Writing the non-negativity of $P(11|11)$ as a Bell inequality gives

$$\vec{B}_8 := \begin{array}{c|c|c} & 0 & 1 \\ \hline 0 & 0 & 0 \\ \hline 1 & 0 & -1 \end{array}, \quad \vec{B}_8\cdot\vec{P} \leqslant \begin{cases} 1 & \mathcal{L} \\ \mathbf{1} & \mathcal{Q} \\ 1 & \mathcal{NS} \end{cases}. \tag{G1}$$

It is easy to verify that the corresponding face of the local set is a (positivity) facet, i.e., a face of maximal dimension. This immediately implies [by inequalities (8) and (9)] that the resulting quantum and no-signaling faces are also of maximal dimension.

While the three faces have the same dimension, they are all different; i.e., the inclusions $\mathcal{F}_{\mathcal{L}} \subsetneq \mathcal{F}_{\mathcal{Q}} \subsetneq \mathcal{F}_{\mathcal{NS}}$ are strict. To see this, observe that the function is saturated by the Hardy point

$$\vec{P}_{\text{Hardy}} := \begin{array}{c|c|c} & 5-2\sqrt{5} & \sqrt{5}-2 \\ \hline 5-2\sqrt{5} & 6\sqrt{5}-13 & 3\sqrt{5}-6 \\ \hline \sqrt{5}-2 & 3\sqrt{5}-6 & 2\sqrt{5}-5 \end{array}, \tag{G2}$$

which is quantum (but nonlocal) and also by the (nonquantum) PR box $\vec{P}_{\text{PR}}$.

As shown in Ref. [58], the Hardy point $\vec{P}_{\text{Hardy}}$ is a self-test and, hence, an extremal point of the quantum set. However, as seen in Fig. 6 and proved in Appendix H, it is not exposed.

It is easy to check that $\vec{P}_{\text{Hardy}}$ saturates two other positivity facets: $P(01|10) \geqslant 0$ and $P(10|01) \geqslant 0$. Thus, $\vec{P}_{\text{Hardy}}$ must also saturate

$$a_1 P(10|01) + a_2 P(01|10) + a_3 P(11|11) \geqslant 0 \tag{G3}$$

for arbitrary $a_1,a_2,a_3 \geqslant 0$, which can be written in terms of expectation values as

$$\vec{B}_9 := \begin{array}{c|c|c} & a_2 & a_3-a_1 \\ \hline a_1 & 0 & a_1 \\ \hline a_3-a_2 & a_2 & -a_3 \end{array},$$

$$\vec{B}_9\cdot\vec{P} \leqslant \begin{cases} a_1+a_2+a_3 & \mathcal{L} \\ \boldsymbol{a_1+a_2+a_3} & \mathcal{Q} \\ a_1+a_2+a_3 & \mathcal{NS} \end{cases}.$$

For $a_1,a_2,a_3 > 0$, the Bell function $\vec{B}_9$ is saturated only by points which simultaneously saturate three positivity facets, corresponding to the three terms in Eq. (G3). Each of the faces identified by Eq. (G3) is thus at most five-dimensional, corresponding to the *intersection* of three seven-dimensional (positivity) faces.

[8] Note that this is not true for slices: It is in general not sufficient to take the convex hull of the extremal points in the slice.

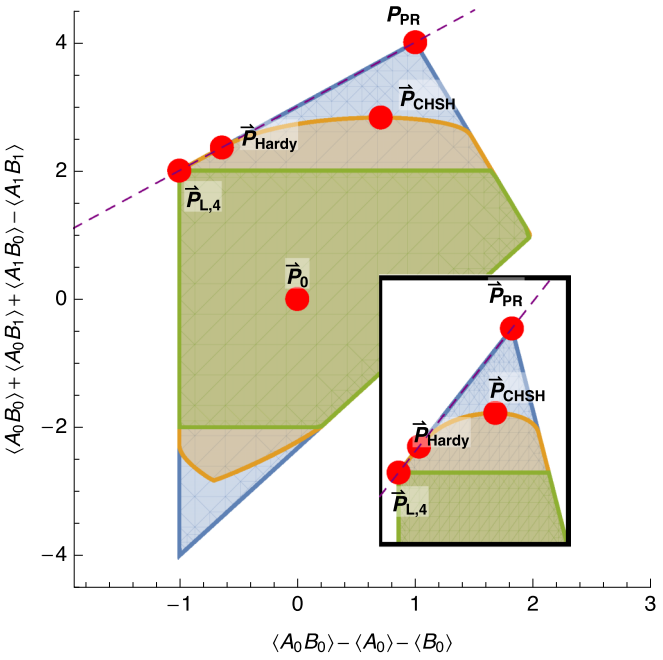

FIG. 6. A slice of the quantum set containing the maximally mixed point $\vec{P}_0$, the PR box $\vec{P}_{\mathrm{PR}}$, and the Hardy point $\vec{P}_{\mathrm{Hardy}}$. The dashed line corresponds to saturating the Bell function $\vec{B}_9$. The point $\vec{P}_{L,4}$ is defined as the intersection of the line going through the PR box and the Hardy point and the hyperplane of the CHSH value of 2. This local point is not deterministic, but it has a unique decomposition in terms of the five deterministic strategies, namely $\vec{P}_{L,4} = \frac{1+2\sqrt{5}}{19}\vec{P}_{d,1} + \frac{9-\sqrt{5}}{38}(\vec{P}_{d,5} + \vec{P}_{d,6} + \vec{P}_{d,7} + \vec{P}_{d,8})$.

It is easy to check that $\vec{B}_9$ is saturated by five local points, namely $\vec{P}_{d,1}$ of Eq. (18) and

$$\vec{P}_{d,5} := \begin{array}{c|c|c} & 1 & -1 \\ \hline 1 & 1 & -1 \\ \hline 1 & 1 & -1 \end{array}, \quad \vec{P}_{d,6} := \begin{array}{c|c|c} & 1 & 1 \\ \hline 1 & 1 & 1 \\ \hline -1 & -1 & -1 \end{array},$$

$$\vec{P}_{d,7} := \begin{array}{c|c|c} & 1 & -1 \\ \hline -1 & -1 & 1 \\ \hline 1 & 1 & -1 \end{array}, \quad \vec{P}_{d,8} := \begin{array}{c|c|c} & -1 & 1 \\ \hline 1 & -1 & 1 \\ \hline -1 & 1 & -1 \end{array}.$$

The local face is the convex hull of these five points and, since they are affinely independent, we obtain a four-dimensional polytope. The Bell function $\vec{B}_9$ is also saturated by the PR box, which implies that the no-signaling face is a five-dimensional polytope. The quantum face corresponding to the Bell function $\vec{B}_9$ contains the five deterministic points and the Hardy point $\vec{P}_{\mathrm{Hardy}}$, so it must be of dimension 5. We do not know, however, whether it is a polytope or not.

APPENDIX H: THE HARDY POINT IS NOT EXPOSED

To prove that the Hardy point $\vec{P}_{\mathrm{Hardy}}$ defined in Eq. (G2) is not exposed in the quantum set, we show that any Bell function $\vec{B}$ maximized by the Hardy point satisfies $\beta_{\mathcal{L}}(\vec{B}) = \beta_{\mathcal{Q}}(\vec{B})$, which implies that the Hardy point is not the unique maximizer.

Rabelo *et al.* showed that the maximal violation of the Hardy paradox self-tests the following two-qubit state and measurements [58]:

$$|\psi_{\mathrm{H}}\rangle = \sqrt{\frac{1-a^2}{2}}\big(|01\rangle + |10\rangle\big) + a|11\rangle,$$
$$A_0 = B_0 = 2a\sigma_x + \sqrt{1-4a^2}\sigma_z,$$
$$A_1 = B_1 = -\sigma_z$$

for $a := \sqrt{\sqrt{5}-2}$. Define operators

$$G_1 = A_0 \otimes \mathbb{1}, \quad G_5 = A_0 \otimes B_0,$$
$$G_2 = A_1 \otimes \mathbb{1}, \quad G_6 = A_0 \otimes B_1,$$
$$G_3 = \mathbb{1} \otimes B_0, \quad G_7 = A_1 \otimes B_0,$$
$$G_4 = \mathbb{1} \otimes B_1, \quad G_8 = A_1 \otimes B_1.$$

Let $\vec{B}$ be an arbitrary Bell function

$$\vec{B} := \begin{array}{c|c|c} & b_3 & b_4 \\ \hline b_1 & b_5 & b_6 \\ \hline b_2 & b_7 & b_8 \end{array}$$

and the corresponding Bell operator equals

$$W = \sum_{j=1}^{8} b_j G_j.$$

If the Bell function $\vec{B}$ is maximized by the Hardy point, then in particular the state $|\psi_{\mathrm{H}}\rangle$ must be an eigenstate of the Bell operator W; i.e., it must satisfy the linear constraint $W|\psi_{\mathrm{H}}\rangle = \lambda|\psi_{\mathrm{H}}\rangle$. This forces the Bell function to be tangent to the boundary of the quantum set at the Hardy point. In the proof, we show that *every* such Bell function is maximized by at least two points: $\vec{P}_{\mathrm{Hardy}}$ and a local point.

The eigenvalue equation $W|\psi_{\mathrm{H}}\rangle = \lambda|\psi_{\mathrm{H}}\rangle$ implies $\langle 00|W|\psi_{\mathrm{H}}\rangle = 0$, because $\langle 00|\psi_{\mathrm{H}}\rangle = 0$. This can be written as a linear constraint $\vec{B}\cdot\vec{T} = 0$, where the entries of $\vec{T}$ are proportional to $\langle 00|G_j|\psi_{\mathrm{H}}\rangle$. More specifically, we set

$$\vec{T} := \begin{array}{c|c|c} & 1 & 0 \\ \hline 1 & \sqrt{5}-1 & -1 \\ \hline 0 & -1 & 0 \end{array}.$$

Our goal is to find the largest value of $\vec{B}\cdot\vec{P}_{\mathrm{Hardy}}$ for a Bell function maximized by the Hardy point. To write this as a linear program, it is convenient to impose some normalization, e.g., that the local bound does not exceed 1 (this is simply a matter of scaling the coefficients). The resulting linear program reads

$$\begin{array}{ll} \max & \vec{B}\cdot\vec{P}_{\mathrm{Hardy}} \\ \text{over} & \vec{B} \in \mathbb{R}^8 \\ \text{subject to} & \vec{B}\cdot\vec{T} = 0 \\ & \vec{B}\cdot\vec{P}_{d,j} \leqslant 1 \ \text{ for } \ j = 1,2,\ldots,16, \end{array}$$

where $\vec{P}_{d,j}$ are the deterministic behaviors.[9] The maximum value of the linear program is found to be identically 1; the optimal Bell function returned by the program is $\vec{B}_8$ as specified

[9]The deterministic behaviors for $j = \{1,2,\ldots,8\}$ were defined in Secs. III B 1, III B 2, and Appendix G 2. The remaining ones turn out to be irrelevant and the corresponding constraints could be removed without affecting the value of the problem.

in Eq. (G1), which achieves no smaller a value at $\vec{P}_{L,4}$ than it does at $\vec{P}_{\text{Hardy}}$, proving that the Hardy point is not exposed.

The optimality of $\vec{B}_8$ can be shown analytically as follows. First, note that $\vec{B}_8$ satisfies the constraints defining the linear program. To further show that $\vec{B}\cdot\vec{P}_{\text{Hardy}} = 1$ is the optimal max-value, we write the dual program

$$\begin{array}{ll} \text{min} & \sum_{k=1}^{16} y_k \\ \text{over} & y_k \geqslant 0,\ z \in \mathbb{R} \\ \text{subject to} & \sum_{k=1}^{16} y_k \vec{P}_{d,j} + z\vec{T} = \vec{P}_{\text{Hardy}}. \end{array}$$

The assignment

$$y_k = \begin{cases} \sqrt{5}-2 & \text{if} \quad k = 1, \\ (3-\sqrt{5})/2 & \text{if} \quad k \in \{5,6\}, \\ 0 & \text{otherwise}, \end{cases}$$

$$z = 4 - 2\sqrt{5},$$

is a valid solution to the dual and the resulting value is 1. This completes the proof that any Bell function maximized by the Hardy point must satisfy $\beta_{\mathcal{L}}(\vec{B}) = \beta_{\mathcal{Q}}(\vec{B})$.

APPENDIX I: THE QUANTUM VALUE OF THE B_6 FUNCTION

Let A_x and B_y denote the observables of Alice and Bob, respectively. The maximal quantum value of the Bell function $\vec{B}_6$ can be determined by finding the maximum eigenvalue of the Bell operator

$$W = A_0(B_0 + B_1 + B_2) + A_1(B_0 + B_1 - B_2) + A_2(B_0 - B_1),$$

where for ease of presentation we assume that A_x and B_y act on the same composite Hilbert space while satisfying the commutation relations $[A_x, B_y] = 0$ for all x, y.

By solving the semidefinite program proposed in Ref. [64], as illustrated in Ref. [78], one essentially obtains a sum-of-squares decomposition for the operator $\gamma\mathbb{1} - W$ for the smallest possible γ, thereby showing that the maximal quantum violation of B_6 is upper bounded by γ. In particular, it is easy to verify that whenever $A_x^2 = B_y^2 = \mathbb{1}$ and the above-mentioned commutation relations hold true, the following holds

$$5 \times \mathbb{1} - W = \frac{1}{2}\sum_{j=1}^{3} V_j^\dagger V_j, \tag{I1}$$

where $V_1 = A_0 + A_1 - B_0 - B_1$, $V_2 = A_0 - A_1 - B_2$, and $V_3 = A_2 - B_0 + B_1$. Since the right-hand side of Eq. (I1) is a non-negative operator, we see that 5 must be an upper bound on the maximal quantum value of B_6. Indeed, this upper bound is saturated by the family of quantum realizations presented in the main text.

APPENDIX J: QUANTUM FACES IN THE TRIPARTITE SCENARIOS

In this appendix, we derive the quantum face corresponding to the Bell function $\vec{B}_8$ discussed in Sec. IV B.

As explained in Appendix A to determine an exposed quantum face, it suffices to find its extremal points. Since these must also be extremal in the entire quantum set, we simply need to find the extremal points of the quantum set which saturate the quantum bound. In a scenario with two binary observables on each site, every extremal point can be obtained by performing projective rank-1 measurements on an n-qubit state [27]. For Alice, we parametrize the observables as

$$A_0 = \sigma_x, \quad A_1 = \cos a \cdot \sigma_x + \sin a \cdot \sigma_y$$

for some angle $a \in [0,\pi]$, while for Bob and Charlie we write

$$B_0 = \cos b \cdot \sigma_x + \sin b \cdot \sigma_y, \quad B_1 = \cos b \cdot \sigma_x - \sin b \cdot \sigma_y,$$
$$C_0 = \cos c \cdot \sigma_x + \sin c \cdot \sigma_y, \quad C_1 = \cos c \cdot \sigma_x - \sin c \cdot \sigma_y.$$

for some angles $b,c \in [0,\pi/2]$. This parametrization ensures that the resulting Bell operator is easy to diagonalize.

The Bell operator corresponding to the Bell function $\vec{B}_8$ can be seen as the CHSH operator

$$W = A_0 \otimes (T_0 + T_1) + A_1 \otimes (T_0 - T_1),$$

where $T_j := B_j \otimes C_j$. This implies that the eigenvalue of $2\sqrt{2}$ is possible only for $a = \pi/2$. Having established the form of Alice's observables, we are ready to find the eigenvectors of W. It is easy to check that

$$T_0 + T_1 = 2(\cos b\, \cos c \cdot \sigma_x \otimes \sigma_x + \sin b\, \sin c \cdot \sigma_y \otimes \sigma_y),$$
$$T_0 - T_1 = 2(\cos b\, \sin c \cdot \sigma_x \otimes \sigma_y + \sin b\, \cos c \cdot \sigma_y \otimes \sigma_x),$$

which implies that

$$\begin{aligned} W|000\rangle &= -2\sqrt{2}\,\sin(b + c - \pi/4)\,|111\rangle, \\ W|001\rangle &= -2\sqrt{2}\,\sin(b - c - \pi/4)\,|110\rangle, \\ W|010\rangle &= 2\sqrt{2}\,\sin(b - c + \pi/4)\,|101\rangle, \\ W|011\rangle &= 2\sqrt{2}\,\sin(b + c + \pi/4)\,|100\rangle, \\ W|100\rangle &= 2\sqrt{2}\,\sin(b + c + \pi/4)\,|011\rangle, \\ W|101\rangle &= 2\sqrt{2}\,\sin(b - c + \pi/4)\,|010\rangle, \\ W|110\rangle &= -2\sqrt{2}\,\sin(b - c - \pi/4)\,|001\rangle, \\ W|111\rangle &= -2\sqrt{2}\,\sin(b + c - \pi/4)\,|000\rangle. \end{aligned}$$

The eigenvectors of W are simply the following GHZ states:

$$\begin{aligned} |\Omega_{\pm 1}\rangle &= \frac{1}{\sqrt{2}}\big(|000\rangle \pm |111\rangle\big), \\ |\Omega_{\pm 2}\rangle &= \frac{1}{\sqrt{2}}\big(|001\rangle \pm |110\rangle\big), \\ |\Omega_{\pm 3}\rangle &= \frac{1}{\sqrt{2}}\big(|010\rangle \pm |101\rangle\big), \\ |\Omega_{\pm 4}\rangle &= \frac{1}{\sqrt{2}}\big(|011\rangle \pm |100\rangle\big), \end{aligned}$$

and the corresponding eigenvalues are

$$\lambda_{\pm 1} = \mp 2\sqrt{2}\,\sin(b + c - \pi/4),$$
$$\lambda_{\pm 2} = \mp 2\sqrt{2}\,\sin(b - c - \pi/4),$$

$$\lambda_{\pm 3} = \pm 2\sqrt{2}\,\sin(b - c + \pi/4),$$
$$\lambda_{\pm 4} = \pm 2\sqrt{2}\,\sin(b + c + \pi/4).$$

Since we are restricted to the square $b,c \in [0,\pi/2]$, the maximum eigenvalue of $2\sqrt{2}$ appears if and only if (at least) one of the following equations is satisfied:

$$b + c = 3\pi/4,$$
$$b - c = -\pi/4,$$
$$b - c = \pi/4,$$
$$b + c = \pi/4.$$

Inside the square, i.e., for $b,c \in (0,\pi)$, the maximum eigenvalue is nondegenerate and the corresponding eigenvector is unique. The one- and two-body marginals of a GHZ state are fully mixed, which implies that the one- and two-body expectation values must vanish:

$$\langle A_x\rangle = \langle B_y\rangle = \langle C_z\rangle = \langle A_x B_y\rangle = \langle A_x C_z\rangle = \langle B_y C_z\rangle = 0.$$

Determining the three-body correlations is a simple exercise. For the branch $b + c = 3\pi/4$, we obtain

$$\langle A_0 B_0 C_0\rangle = \langle A_0 B_1 C_1\rangle = -\cos(b + c) = \frac{1}{\sqrt{2}},$$
$$\langle A_0 B_0 C_1\rangle = \langle A_0 B_1 C_0\rangle = -\cos(b - c),$$
$$\langle A_1 B_0 C_0\rangle = -\langle A_1 B_1 C_1\rangle = \sin(b + c) = \frac{1}{\sqrt{2}},$$
$$\langle A_1 B_0 C_1\rangle = -\langle A_1 B_1 C_0\rangle = \sin(b - c),$$

which corresponds to Eq. (32) for $\alpha \in [3\pi/4,5\pi/4]$. The other branches give analogous results and cover the rest of the range.

To complete the analysis, we must also look at the four special points where the maximal eigenvalue is degenerate, i.e., $(b,c) = (\pi/4,0),(0,\pi/4),(\pi/2,0)$, and $(0,\pi/2)$. At each of these points, the subspace corresponding to the maximal eigenvalue is two-dimensional and the resulting statistics form a line; i.e., we obtain two extremal points. Computing the extremal points for each pair (b,c) yields the eight points $\{P_j\}_{j=1}^{8}$ presented in the main text.

[1] J. S. Bell, On the Einstein-Podolsky-Rosen paradox, Physics **1**, 195 (1964).

[2] B. Hensen, H. Bernien, A. E. Dréau, A. Reiserer, N. Kalb, M. S. Blok, J. Ruitenberg, R. F. L. Vermeulen, R. N. Schouten, C. Abellán *et al.*, Loophole-free Bell inequality violation using electron spins separated by 1.3 kilometres, Nature (London) **526**, 682 (2015).

[3] L. K. Shalm, E. Meyer-Scott, B. G. Christensen, P. Bierhorst, M. A. Wayne, M. J. Stevens, T. Gerrits, S. Glancy, D. R. Hamel, M. S. Allman *et al.*, Strong Loophole-Free Test of Local Realism, Phys. Rev. Lett. **115**, 250402 (2015).

[4] M. Giustina, M. A. M. Versteegh, S. Wengerowsky, J. Handsteiner, A. Hochrainer, K. Phelan, F. Steinlechner, J. Kofler, J.-A. Larsson, C. Abellán *et al.*, Significant-Loophole-Free Test of Bell's Theorem with Entangled Photons, Phys. Rev. Lett. **115**, 250401 (2015).

[5] W. Rosenfeld, D. Burchardt, R. Garthoff, K. Redeker, N. Ortegel, M. Rau, and H. Weinfurter, Event-Ready Bell Test Using Entangled Atoms Simultaneously Closing Detection and Locality Loopholes, Phys. Rev. Lett. **119**, 010402 (2017).

[6] N. Brunner, D. Cavalcanti, S. Pironio, V. Scarani, and S. Wehner, Bell nonlocality, Rev. Mod. Phys. **86**, 419 (2014).

[7] J. F. Clauser, M. A. Horne, A. Shimony, and R. A. Holt, Proposed Experiment to Test Local Hidden-Variable Theories, Phys. Rev. Lett. **23**, 880 (1969).

[8] N. D. Mermin, Extreme Quantum Entanglement in a Superposition of Macroscopically Distinct States, Phys. Rev. Lett. **65**, 1838 (1990).

[9] S. Popescu and D. Rohrlich, Quantum nonlocality as an axiom, Found. Phys. **24**, 379 (1994).

[10] B. Tsirelson, Some results and problems on quantum Bell-type inequalities, Hadronic J. Suppl. **8**, 329 (1993).

[11] S. Pironio, Lifting Bell inequalities, J. Math. Phys. **46**, 062112 (2005).

[12] C. Branciard, Detection loophole in Bell experiments: How postselection modifies the requirements to observe nonlocality, Phys. Rev. A **83**, 032123 (2011).

[13] J. Allcock, N. Brunner, M. Pawłowski, and V. Scarani, Recovering part of the boundary between quantum and nonquantum correlations from information causality, Phys. Rev. A **80**, 040103 (2009).

[14] J. Allcock, N. Brunner, N. Linden, S. Popescu, P. Skrzypczyk, and T. Vértesi, Closed sets of nonlocal correlations, Phys. Rev. A **80**, 062107 (2009).

[15] M. L. Almeida, J.-D. Bancal, N. Brunner, A. Acín, N. Gisin, and S. Pironio, Guess your Neighbor's Input: A Multipartite Nonlocal Game with no Quantum Advantage, Phys. Rev. Lett. **104**, 230404 (2010).

[16] T. H. Yang, M. Navascués, L. Sheridan, and V. Scarani, Quantum Bell inequalities from macroscopic locality, Phys. Rev. A **83**, 022105 (2011).

[17] T. Fritz, A. B. Sainz, R. Augusiak, J. Brask, R. Chaves, A. Leverrier, and A. Acín, Local orthogonality as a multipartite principle for quantum correlations, Nat. Commun. **4**, 2263 (2013).

[18] G. Pütz, D. Rosset, T. J. Barnea, Y.-C. Liang, and N. Gisin, Arbitrarily Small Amount of Measurement Independence is Sufficient to Manifest Quantum Nonlocality, Phys. Rev. Lett. **113**, 190402 (2014).

[19] R. Chaves, C. Majenz, and D. Gross, Information-theoretic implications of quantum causal structures, Nat. Commun. **6**, 5766 (2015).

[20] J. I. de Vicente, Simple conditions constraining the set of quantum correlations, Phys. Rev. A **92**, 032103 (2015).

[21] B. G. Christensen, Y.-C. Liang, N. Brunner, N. Gisin, and P. G. Kwiat, Exploring the Limits of Quantum Nonlocality with Entangled Photons, Phys. Rev. X **5**, 041052 (2015).

[22] P.-S. Lin, D. Rosset, Y. Zhang, J.-D. Bancal, and Y.-C. Liang, Device-independent point estimation from finite data, arXiv:1705.09245.

[23] Y. Zhou, Y. Cai, J.-D. Bancal, F. Gao, and V. Scarani, Many-box locality, Phys. Rev. A **96**, 052108 (2017).

[24] B. S. Tsirelson, Quantum analogues of the Bell inequalities. The case of two spatially separated domains, J. Sov. Math. **36**, 557 (1987).

[25] L. J. Landau, Empirical two-point correlation functions, Found. Phys. **18**, 449 (1988).

[26] R. F. Werner and M. M. Wolf, All-multipartite Bell-correlation inequalities for two dichotomic observables per site, Phys. Rev. A **64**, 032112 (2001).

[27] L. Masanes, Asymptotic Violation of Bell Inequalities and Distillability, Phys. Rev. Lett. **97**, 050503 (2006).

[28] A. Cabello, How much larger quantum correlations are than classical ones, Phys. Rev. A **72**, 012113 (2005).

[29] I. Pitowsky, *Quantum Probability—Quantum Logic*, 1st ed., Lecture Notes in Physics Vol. 321 (Springer-Verlag, Berlin, 1989).

[30] M. Navascués and H. Wunderlich, A glance beyond the quantum model, Proc. R. Soc. A **466**, 881 (2010).

[31] M. Pawłowski, T. Paterek, D. Kaszlikowski, V. Scarani, A. Winter, and M. Żukowski, Information causality as a physical principle, Nature (London) **461**, 1101 (2009).

[32] M. Navascués, Y. Guryanova, M. J. Hoban, and A. Acín, Almost quantum correlations, Nat. Commun. **6**, 6288 (2015).

[33] S. Popescu and D. Rohrlich, Which states violate Bell's inequality maximally? Phys. Lett. A **169**, 411 (1992).

[34] D. Mayers and A. Yao, Self-testing quantum apparatus, Quantum Inf. Comput. **4**, 273 (2004).

[35] L. Hardy, Quantum Mechanics, Local Realistic Theories, and Lorentz-Invariant Realistic Theories, Phys. Rev. Lett. **68**, 2981 (1992).

[36] J. M. Donohue and E. Wolfe, Identifying nonconvexity in the sets of limited-dimension quantum correlations, Phys. Rev. A **92**, 062120 (2015).

[37] M. Navascués, S. Pironio, and A. Acín, A convergent hierarchy of semidefinite programs characterizing the set of quantum correlations, New J. Phys. **10**, 073013 (2008).

[38] J. Barrett, N. Linden, S. Massar, S. Pironio, S. Popescu, and D. Roberts, Nonlocal correlations as an information-theoretic resource, Phys. Rev. A **71**, 022101 (2005).

[39] J. Barrett and S. Pironio, Popescu-Rohrlich Correlations as a Unit of Nonlocality, Phys. Rev. Lett. **95**, 140401 (2005).

[40] A. Acín, T. Fritz, A. Leverrier, and A. B. Sainz, A combinatorial approach to nonlocality and contextuality, Commun. Math. Phys. **334**, 533 (2015).

[41] N. S. Jones and L. Masanes, Interconversion of nonlocal correlations, Phys. Rev. A **72**, 052312 (2005).

[42] H. Barnum, S. Beigi, S. Boixo, M. B. Elliott, and S. Wehner, Local Quantum Measurement and No-Signaling Imply Quantum Correlations, Phys. Rev. Lett. **104**, 140401 (2010).

[43] W. Slofstra, The set of quantum correlations is not closed, arXiv:1703.08618.

[44] K. Dykema, V. I. Paulsen, and J. Prakash, Non-closure of the set of quantum correlations via graphs, arXiv:1709.05032.

[45] D. Rosset, J.-D. Bancal, and N. Gisin, Classifying 50 years of Bell inequalities, J. Phys. A: Math. Theo. **47**, 424022 (2014).

[46] R. Ramanathan, J. Tuziemski, M. Horodecki, and P. Horodecki, No Quantum Realization of Extremal No-Signaling Boxes, Phys. Rev. Lett. **117**, 050401 (2016).

[47] R. Cleve, P. Høyer, B. Toner, and J. Watrous, Consequences and limits of nonlocal strategies, in *Proceedings of the 19th IEEE Annual Conference on Computational Complexity, 2004* (IEEE, Piscataway, NJ, 2004).

[48] A. Fine, Hidden Variables, Joint Probability, and the Bell Inequalities, Phys. Rev. Lett. **48**, 291 (1982).

[49] Y.-C. Liang, N. Harrigan, S. D. Bartlett, and T. Rudolph, Nonclassical Correlations from Randomly Chosen Local Measurements, Phys. Rev. Lett. **104**, 050401 (2010).

[50] V. Scarani, Local and nonlocal content of bipartite qubit and qutrit correlations, Phys. Rev. A **77**, 042112 (2008).

[51] P. Bierhorst, Geometric decompositions of Bell polytopes with practical applications, J. Phys. A: Math. Theor. **49**, 215301 (2016).

[52] M. McKague, T. H. Yang, and V. Scarani, Robust self-testing of the singlet, J. Phys. A **45**, 455304 (2012).

[53] J.-D. Bancal, *On the Device-Independent Approach to Quantum Physics* (Springer, Berlin, 2014).

[54] E. Wolfe and S. F. Yelin, Quantum bounds for inequalities involving marginal expectation values, Phys. Rev. A **86**, 012123 (2012).

[55] L. Masanes, Extremal quantum correlations for N parties with two dichotomic observables per site, arXiv:quant-ph/0512100.

[56] B. S. Cirel'son, Quantum generalizations of Bell's inequality, Lett. Math. Phys. **4**, 93 (1980).

[57] Y. Wang, X. Wu, and V. Scarani, All the self-testings of the singlet for two binary measurements, New J. Phys. **18**, 025021 (2016).

[58] R. Rabelo, Y. Z. Law, and V. Scarani, Device-Independent Bounds for Hardy's Experiment, Phys. Rev. Lett. **109**, 180401 (2012).

[59] L. Mančinska and S. Wehner, A unified view on Hardy's paradox and the Clauser-Horne-Shimony-Holt inequality, J. Phys. A: Math. Theor. **47**, 424027 (2014).

[60] W. Slofstra, Lower bounds on the entanglement needed to play XOR non-local games, J. Math. Phys. **52**, 102202 (2011).

[61] R. Ramanathan and P. Mironowicz, Trade-offs in multi-party Bell inequality violations in qubit networks, arXiv:1704.03790.

[62] M. Froissart, Constructive generalization of Bell's inequalities, Nuovo Cimento B **64**, 241 (1981).

[63] D. Collins and N. Gisin, A relevant two qubit Bell inequality inequivalent to the CHSH inequality, J. Phys. A: Math. Gen. **37**, 1775 (2004).

[64] S. Wehner, Tsirelson bounds for generalized Clauser-Horne-Shimony-Holt inequalities, Phys. Rev. A **73**, 022110 (2006).

[65] M. McKague and M. Mosca, Generalized self-testing and the security of the 6-state protocol, in *Theory of Quantum Computation, Communication, and Cryptography*, edited by W. van Dam, V. M. Kendon, and S. Severini (Springer, Berlin, Heidelberg, 2010), Chap. 11, pp. 113–130.

[66] O. Andersson, P. Badziąg, I. Bengtsson, I. Dumitru, and A. Cabello, Self-testing properties of Gisin's elegant Bell inequality, Phys. Rev. A **96**, 032119 (2017).

[67] J. Kaniewski, Self-testing of binary observables based on commutation, Phys. Rev. A **95**, 062323 (2017).

[68] R. Colbeck, Quantum and relativistic protocols for secure multi-party computation, Ph.D. thesis, University of Cambridge, Cambridge, UK, 2006, arXiv:0911.3814.

[69] K. F. Pál, T. Vértesi, and M. Navascués, Device-independent tomography of multipartite quantum states, Phys. Rev. A **90**, 042340 (2014).

[70] S. Pironio, J.-D. Bancal, and V. Scarani, Extremal correlations of the tripartite no-signaling polytope, J. Phys. A **44**, 065303 (2011).

[71] T. Krisnanda, M. Zuppardo, M. Paternostro, and T. Paterek, Revealing Nonclassicality of Inaccessible Objects, Phys. Rev. Lett. **119**, 120402 (2017).

[72] C. Śliwa, Symmetries of the Bell correlation inequalities, Phys. Lett. A **317**, 165 (2003).

[73] D. M. Greenberger, M. A. Horne, and A. Zeilinger, Going beyond Bell's theorem, in *Bell's Theorem, Quantum Theory and Conceptions of the Universe*, Fundamental Theories of Physics, Vol. 37, edited by M. Kafatos (Springer, Dordrecht, 1989).

[74] B. Simon, *Convexity: An Analytic Viewpoint* (Cambridge University Press, Cambridge, UK, 2011).

[75] A. Basu, G. Cornuéjols, and G. Zambelli, Convex sets and minimal sublinear functions, J. Convex Analysis **18**, 427 (2011).

[76] T. H. Yang and M. Navascués, Robust self-testing of unknown quantum systems into any entangled two-qubit states, Phys. Rev. A **87**, 050102(R) (2013).

[77] C. Bamps and S. Pironio, Sum-of-squares decompositions for a family of Clauser-Horne-Shimony-Holt-like inequalities and their application to self-testing, Phys. Rev. A **91**, 052111 (2015).

[78] A. C. Doherty, Y.-C. Liang, B. Toner, and S. Wehner, The quantum moment problem and bounds on entangled multi-prover games, in *Proceedings of the 2008 IEEE 23rd Annual Conference on Computational Complexity, CCC '08* (IEEE Computer Society, Washington, DC, 2008), p. 199.